

New User Event Prediction Through the Lens of Causal Inference

Henry Shaowu Yuchi¹ and Shixiang Zhu²

¹Los Alamos National Laboratory

²Carnegie Mellon University

Abstract

Modeling and analysis for event series generated by heterogeneous users of various behavioral patterns are closely involved in our daily lives, including credit card fraud detection, online platform user recommendation, and social network analysis. The most commonly adopted approach to this task is to classify users into behavior-based categories and analyze each of them separately. However, this approach requires extensive data to fully understand user behavior, presenting challenges in modeling newcomers without historical knowledge. In this paper, we propose a novel discrete event prediction framework for new users through the lens of causal inference. Our method offers an unbiased prediction for new users without needing to know their categories. We treat the user event history as the “treatment” for future events and the user category as the key confounder. Thus, the prediction problem can be framed as counterfactual outcome estimation, with the new user model trained on an adjusted dataset where each event is re-weighted by its inverse propensity score. We demonstrate the superior performance of the proposed framework with a numerical simulation study and two real-world applications, including Netflix rating prediction and seller contact prediction for customer support at Amazon.

1 Introduction

Event prediction has always been closely intertwined with our daily life. It refers to forecasting the occurrence of events in the future based on knowledge of the past and the present. This process necessitates estimating the time, the location, and the nature of the upcoming incident. Practically, numerous daily activities revolve around the concept of event prediction. For instance, credit card fraud detection is an everyday scenario where transactions significantly deviating from predicted user behaviors are flagged [12, 37, 84]. Other examples include predicting airline flight disruption to alleviate delays [35], mobile user action to enhance service [48], landslide hazard prediction to prevent life and property losses [60], and oil wells incidents to improve operation safety [47].

In this new era of e-commerce, social media, and the Internet of Things [38], event prediction for individual users on these platforms is becoming more relevant and critical than ever. The sheer scale of users and the amount of their event data lead to unprecedented challenges for user event prediction. During the year 2023, Facebook amassed a monthly active user base of over 3 billion people [33], eBay users traded an annual merchandise value of over 73 billion US dollars [19], and more than 5 billion Snaps were created daily by Snapchat users on average [34]. Predicting user events on such a massive scale is highly complex and difficult.

To address this complexity, users are often grouped based on similar properties or historical behavior, a practice common on many online platforms [63]. However, these platforms face high user turnover, with many users quickly becoming inactive – a phenomenon known as “user churning” [6, 79]. For example, a study [20] on Twitter found that a quarter of new users planned to take a break within a year, and newer users, including those returning from a hiatus, were twice as likely to leave the platform. Similarly, the new social media platform Threads by Meta saw roughly 75% of its 2.3 million daily active users in the United States become inactive within a month of its launch [10]. This indicates that new users are transient and their behavior is highly dynamic.

Consequently, new users often receive insufficient attention in event prediction. On one hand, it is impractical to apply a single uniform model to both new and existing users due to their heterogeneous behaviors. On the other hand, categorizing new users is challenging as it typically requires extensive user properties and features extracted from their activities over a long period [63]. This often leads to a lack of category information for relatively new users, which is crucial in addressing their unique needs, causing significant performance discrepancies between different user groups. The main issues arise from the absence of category information for new users due to their short exposure to the service, resulting in several challenges: (i) The absence of category information causes confounding bias to the event prediction due to the complex dependencies between future behavior, historical events, and user categories, resulting in modeling distortions. (ii) The distribution of user events across categories is imbalanced. Without category information, modeling user events tend to favor categories with more users or more data.

A motivating example that we look into in this work is event predictions for third-party selling partners on Amazon. On their online marketplace, millions of different users (third-party sellers) frequently need to contact the platform support representatives when they encounter issues operating on the e-commerce platform. The issues can be wide-ranging, including inventory updates, storefront construction, account verification, procurement contracting, buyer disputes, and so on. The time of the requests from users is automatically recorded, and the Amazon user support representatives will work with the users to resolve their issues or concerns after identifying the purpose of the request event and assigning a designated “intent” to it selected from a set of potential choices. This enables the representatives to quickly locate the corresponding streamlined procedure to help the users. Therefore, this user contact intent prediction problem becomes crucial for the business as it heavily impacts the support system efficiency [15]. However, the volume of user contact events tends to vary significantly and unexpectedly, and the behavior between different users varies considerably, creating challenges for Amazon to prepare for the necessary support capacity. To improve efficiency, the platform has been categorizing known users into several groups, assigning

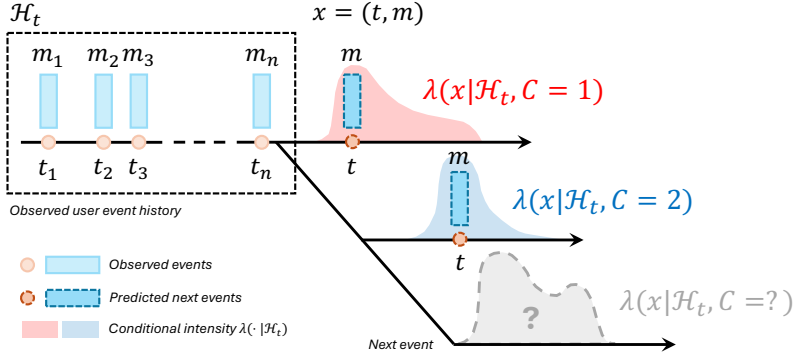


Figure 1: The goal is to predict the next event for a new user without knowing its category. The distribution of the next event is influenced by its category even with the same event history. Each event x consists of its occurrence time t and associated mark data m . The conditional intensity $\lambda(x|\mathcal{H}_t, C)$ represents the occurrence rate of the next event x given its history \mathcal{H}_t and the user's category C .

category information to each of them such that the representatives are more familiar with the typical user contacts and do not have to start from scratch. In practice, this is conducted by experienced support professionals involving collecting extensive background information, past behavior, user context, and more, and it is a time-consuming manual process. To further improve the service quality for the users, the platform is looking into automating the support service by conducting forecast on potential issues from users and providing self-service help to the best quality in addition to the representatives.

To address these challenges, we formulate a *new user event prediction* problem, as illustrated in Fig. 1. Specifically, we investigate the problem by asking a “what if” question, *i.e.*, “When would the next event occur and what would be the mark of the next event given this new user had engaged in a series of activities, without knowing the user’s category?” We answer this question by *viewing a user’s event history as a form of “intervention” to its next event and its category as the “confounder”*. The objective is to study the causal effect from certain history across the entire user base, irrespective of each user’s specific category. This is achieved through reweighting the observed user event sequences with category information. The weights are motivated by the inverse propensity score from causal inference, which is the inverse probability of a user having a specific history record given their observed characteristics. This is equivalent to asking that “Provided what is known about the user, how likely they will be given the corresponding event history (treatment)”. Inverse propensity scoring is utilized to balance users based on their propensity scores, giving more weight to those underrepresented otherwise in the model. This makes event prediction unbiased given the heterogeneous behavior of multiple users. In sum, the main contributions of this paper are threefold:

1. This work enables event prediction for new users without the necessity for their category information which is hard to acquire.
2. This work aims to achieve unbiased user event prediction through a novel counterfactual framework by viewing the user’s history as the intervention to its future event.

3. It is demonstrated in this paper that the proposed framework can achieve superior performance with both simulation studies and real applications, validating the potential of the method to be more widely implemented.

This work is organized as follows: We first survey a few subjects related to this work in Section 2, including point process models with neural networks, causal inference, and studies into new user behavior. We then lay out the preliminary formulation for marked temporal point processes including the prominent neural point process models in Section 3. We proceed to detail the proposed counterfactual intensity framework including the inverse propensity re-weighting, the conditional history transition schemes, and the sensitivity analysis in Section 4. In Section 5.1, we demonstrate the performance of the proposed framework with a comprehensive simulation study compared against several state-of-the-art baseline methods. Then in Section 5.2, we investigate two real-world user event prediction applications, including the motivating example of Amazon customer contact intent prediction. Finally, we summarize our findings in Section 6.

2 Related works

Point process models have been a powerful and popular tool used for discrete event prediction with a wide range of applications, including earthquake prediction [58, 71], crime modeling [53, 54, 83], infectious disease forecasting [13, 25], business warranty claims [74], and social network studies [24, 77]. Especially, temporal point process models have been widely applied for user event prediction in e-commerce [26, 49] given history, as the online marketplace has been rapidly gaining popularity over recent years. The versatile use of point process models shown in these demanding problems indicates their prowess in tackling complex datasets and rooting out intricate relations buried among the data.

The seminal work by [29] introduced the concept of the self-exciting temporal Hawkes point process. A similar self-correcting point process was introduced in [59]. Spatio-temporal point process models extend the event space of observations to include location [14]. Point process models have been thoroughly reviewed in [14, 44, 64]. There have been attempts at event prediction for multiple users given past sequences. The work by [18] establishes a user-item-event framework utilizing a self-exciting Hawkes point process model and exploits the low-rank property of the data. However, in the problem pursued by this work, users' behavior is highly heterogeneous when there are many of them, which no longer satisfies the low-rank assumption.

With the rise to prominence of neural networks (NN) that can model intricate and complex relationships between events, it has been taken up to further enhance the expressiveness of point process models. We introduce two such major research efforts. The first one is the Neural Hawkes process (NH) proposed by [51], which is a self-modulating multivariate point process. It models the the conditional intensity function using a neural network constructed with a high-dimensional hidden state variable which in turn depends on another set of memory variables in continuous-time Long Short Term Memory (LSTM) [27]. The other work is the Recurrent Marked Temporal Point Process (RMTPP) proposed in [17], where the event history is encoded using a hidden embedding layer pushed through a recurrent neural network (RNN). In both works, the utilization of the hidden history layer in NN facilitates the encapsulation of past event

information. Other similar works include modeling the conditional intensity also using RNN [81] and reinforcement learning [46].

Our work is closely connected to the topic of causal inference, which has garnered growing interest in recent years. Classic approaches to analyzing time-varying treatment effects include the marginal structural models [67, 68, 69], while other approaches utilize the g-formula and structural nested models [65, 66, 70]. These pioneering works typically construct parametric models for the treatment effects, which are straightforward but relatively less flexible. In this work, we regard the history embedding as the treatment/intervention variable to be estimated, which can be continuous [87] or of high dimension [86].

Though our work aims to improve automatic event prediction for new users, it differs from the concept of counterfactual fairness and equal opportunity. Causal inference is related to the concept of counterfactual fairness and equal opportunity. Counterfactual fairness means decision-making is conditionally independent from sensitive attributes such as demographics given the rest [42], following the causal model by [62]. Equal opportunity indicates the distribution of the decision remains the same however the sensitive attributes change [28]. The study by [76] utilizes this method to achieve equal bias across different groups. However, fair learning typically assumes the knowledge of the sensitive attributes, which is not the case here, and therefore not applicable.

Instead of directly aiming for counterfactual fairness, we elect to pursue unbiased prediction via the history embedding variable using causal inference. We regard it as the treatment/intervention variable, which is closely related to effect treatment estimation. There is flexibility in configuring the treatment effects. Treatment variables can be continuous [87] and of higher dimension [86]. Recently, new efforts have been made in this direction. Now treatment effects can be estimated in several ways, including by spline and kernel regression [39, 57], Gaussian process [11, 72], RNN-based models [45, 50], adversarial networks [7, 80], and transformer models [52]. Apart from that, Bayesian inference has been applied to obtain precision/accuracy in estimating heterogeneous effects [3, 4], enabling uncertainty quantification with effect estimation. Estimation errors can be validated via influence functions as well [2]. Additionally, causally-aware imputation may assist with estimating missing data corresponding to the underlying mechanism [43]. A generative model producing counterfactual samples has been proposed as well [78].

Understanding the behavior of new users on various platforms and networks is pertinent to the effort in this work. The work by [9] studied the behavior of new users on social networks for motivating factors that keep them going. Interpretable clustering for new users on social networks based on user features, network properties, and user behavior is proposed in [79], which looks into new user churn prediction utilizing a sequence-to-sequence model leveraging LSTM. The work by [31] attempts to carry out user clustering from behavior profile, which includes new users as well. The new user problem has also been extensively studied in collaborative filtering [1, 8]. It is often treated as a cold start problem with less or even no event information from new users [36] and the performance from different recommender systems vary [40]. There are primarily two types of approaches to this problem, including constructing useful similarity metrics [1, 8, 75] and leveraging additional user profile information [21, 23]. However, these works generally conduct modeling of new user behavior by appropriating it to the behavior of more matured users, which do not take into account the fact that

it can be challenging to establish category information for new users and then construct prediction models.

3 Preliminaries

The proposed event prediction framework utilizes marked temporal point process and neural point process as its key pieces. We introduce their structures and notations in this section, laying the foundation for the framework. Additionally, we introduce the Markov history property central to the proposed framework.

Marked temporal point processes Marked temporal point processes (MTPPs) [64] consist of a sequence of *discrete events* over time. Each event is associated with a *mark* that contains detailed information about the event, such as user intent in our case study. Let $T > 0$ be a fixed time-horizon, and $\mathcal{M} \subseteq \mathbb{R}^d$ be the space of marks. We denote the space of observation by $\mathcal{X} = [0, T) \times \mathcal{M}$ and the i th data point in the discrete event sequence by

$$x_i = (t_i, m_i), \quad t_i \in [0, T), \quad m_i \in \mathcal{M},$$

where t_i is the event time and m_i represents the corresponding mark. Let N_t be the number of events up to time $t < T$ (which is random). We define $\mathcal{H}_t := \{x_1, x_2, \dots, x_{N_t}\}$, denoting historical events. Let \mathbb{N} be the counting measure on \mathcal{X} , *i.e.*, for any measurable $S \subseteq \mathcal{X}$, $\mathbb{N}(S) = |\mathcal{H}_t \cap S|$. For any function $g : \mathcal{X} \rightarrow \mathbb{R}$, the integral with respect to the counting measure is defined as

$$\int_S g(x) d\mathbb{N}(x) = \sum_{x_i \in \mathcal{H}_T \cap S} g(x_i).$$

The distribution of events in MTPPs is typically characterized via the conditional intensity function λ , which is defined to be the occurrence rate of events in the marked temporal space \mathcal{X} given the events' history $\mathcal{H}_{t(x)}$, *i.e.*,

$$\lambda(x|\mathcal{H}_{t(x)}) = \mathbb{E} (d\mathbb{N}(x)|\mathcal{H}_{t(x)}) / dx, \quad (1)$$

where $t(x)$ extracts the occurrence time of the possible event x . Given the conditional intensity function λ , the corresponding conditional probability density function (PDF) can be expressed as

$$f(x|\mathcal{H}_{t(x)}) = \lambda(x|\mathcal{H}_{t(x)}) \cdot \exp \left(- \int_{[t_n, t(x)) \times \mathcal{M}} \lambda(u|\mathcal{H}_{t(u)}) du \right), \quad (2)$$

where t_n denotes the time of the most recent event that occurred before time $t(x)$.

The point process models can be fitted using maximum likelihood estimation (MLE). The log-likelihood of observing a sequence with N_T events can therefore be obtained by

$$\ell(x_1, \dots, x_{N_T}) = \int_{\mathcal{X}} \log \lambda(x|\mathcal{H}_{t(x)}) d\mathbb{N}(x) - \int_{\mathcal{X}} \lambda(x|\mathcal{H}_{t(x)}) dx. \quad (3)$$

See the derivations in Appendix A.

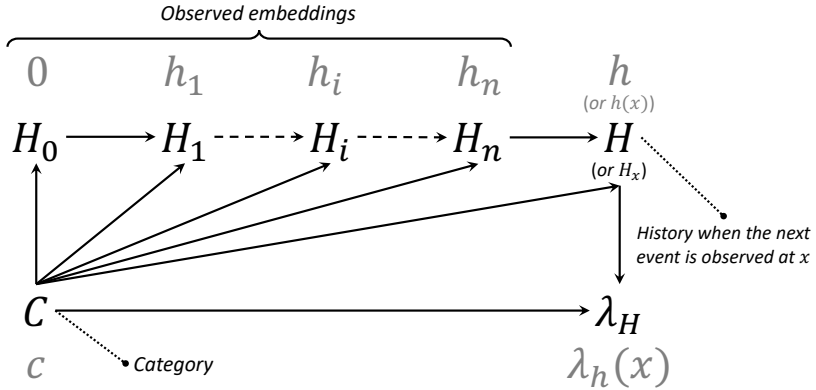


Figure 2: Causal DAG between user category, history variables, and counterfactual intensity. The lowercase notations represent the realizations of these variables. We use n to denote the number of observed events in the history and $h(x)$ (or simply h) denotes the history when we observe the next $(n + 1)$ -th event at x .

Neural point processes Neural point processes (NPPs) [17, 51, 88] are commonly used for modeling complex event sequences. In NPPs, the event history is summarized using a *history encoder*, often a recursive structure such as recurrent neural networks (RNNs) [17, 51] or Transformers [85, 88], taking the history of event x as its input and generating a low-dimensional and compact *history embedding*, denoted by $h(x) \in \mathcal{H} \subseteq \mathbb{R}^q$. This history embedding represents an updated summary of the past events including x . Assume there are n observed events for a user, the history embedding of the next event x , $h(x)$, can be written as follows:

$$h(x) = \phi(t(x) - t(x_n), m(x), h(x_n)), \quad (4)$$

where ϕ is a non-linear mapping, and n denotes the index of the last observed event before $t(x)$. Therefore, the conditional intensity in (1) can be approximated/modeled by

$$\lambda(x|\mathcal{H}_{t(x)}) \approx \lambda_\theta(x|h(x)), \quad (5)$$

where θ denotes the parameters of the model, including the parameters in λ and the nonlinear mapping ϕ . The corresponding conditional PDF can then be denoted by f_θ following (2).

4 New user event prediction

In this section, we discuss the next-event prediction problem for a new user and propose a novel event prediction framework through the lens of causal inference. The objective is to find an approach that enables unbiased prediction of the next immediate event \hat{x}_{n+1} for a new user based on their history $h(x)$ without the knowledge of the particular new user’s category information C . We relay the counterfactual framework and the IPTW reweighting scheme.

4.1 Counterfactual event intensity estimation

By viewing the event history $h(x)$ as the intervention and the user category C as the confounder, our goal is to provide an unbiased estimation of the effect of event history

$h(x)$ on the next event x , while accounting for the influence of the confounding variable C . We first introduce a new notion that treats the history embedding as a random variable, termed *random history variable*:

Definition 1 (Random history variable). *The history embedding h_i and $h(x)$ are considered realizations of two random variables, denoted by H_i and H_x , respectively, and collectively referred to as history variables. We note that H_x depends on H_n and H_i depends on H_{i-1} according to (4).*

Further, we show that history variables possess the Markov property [41]:

Lemma 1 (Markov property). *The history embedding h_0, h_1, \dots, h_i , and $h(x)$ possess the Markov property, formulated as follows:*

$$\lambda(x|h(x)) = \lambda(x|h(x), h_n, \dots, h_i, \dots, h_1, h_0). \quad (6)$$

This can be shown from the definition of $h(x)$ in (4), where $h(x)$ can be specified by x and h_n .

For more details and the proof on the Markov property, see Appendix B. Our proposed approach is grounded in Lemma 1 that the history variable of a user is influenced by both the previous history and its user category, leading to the following definition:

Definition 2 (Dependence of users' future event). *The immediate next event of a user is not only affected by its up-to-date history H_x reflected in (5), but also by the user's category C . The causal directed acyclic graph (DAG) of these variables is shown in Fig. 2.*

We refer to our estimand as *counterfactual intensity*, which is formally defined as follows:

Definition 3 (Counterfactual intensity). *The counterfactual occurrence rate of the next event x , given a user has already taken the first n activities represented by $H = h$, can be defined by*

$$\lambda_h(x) = \mathbb{E}(d\mathbb{N}_h(x)) / dx,$$

where $\mathbb{N}_h(x)$ is the counting measure of a user if the user "receives" history h .

We note that the counterfactual intensity $\lambda_h(x)$ describes the interventional distribution of the next event, assuming the same event history across all users. This is notably different from the unadjusted conditional intensity $\lambda(x|h)$, which does not factor in the disparity of users' category across the entire population. To identify the counterfactual intensity, we state the following three key assumptions:

1. *Consistency*: Provided the history is h , then $\lambda_h(x)$ is the potential intensity under history h . Formally, $H = h \Rightarrow \lambda(x|H = h) = \lambda_h(x)$.
2. *Positivity*: If $\mathbb{P}(H_i = h_i, H_{i-1} = h_{i-1}, C = c) \neq 0$, then $\mathbb{P}(H_i = h_i | H_{i-1} = h_{i-1}, C = c) > 0$ for all $h_i, h_{i-1} \in \mathcal{H}$ [32].
3. *Unconfoundedness*: For all $h \in \mathcal{H}$ and $c \in \mathcal{C}$, $\lambda_h(x) \perp\!\!\!\perp H | C = c$. Armed with this assumption, we can identify the causal effect within values of C using adjustment formula [56], *i.e.*,

$$\lambda_h(x) = \mathbb{E}_C [\lambda(x|H = h, C)].$$

Assumption 2 indicates that, for each event, each possible history has a non-zero probability of being assigned. Assumption 3, also called conditional exchangeability, means there are no unmeasured confounders. The user category is the only variable affecting both the treatment assignment and the next event that is present in the observational data set. Note that while assumption 3 is standard across all methods for estimating treatment effects, it is not testable in practice [61, 69].

Inverse propensity re-weighting Rather than directly analyzing the counterfactual intensity, λ_h , our approach instead starts with establishing the *counterfactual probability density*, f_h , for the next event. This idea is summarized in the following Lemma 2, which is based on the principle of inverse propensity treatment weight (IPTW) inspired by [22, 67, 78]:

Lemma 2 (Counterfactual probability density). *Under unconfoundedness and positivity assumptions, the counterfactual probability density function of the next event x with its history h is defined as*

$$f_h(x) = \sum_{c \in \mathcal{C}} \frac{1}{\prod_{i=1}^{n+1} f(h_i|h_{i-1}, c)} f(x, h, c) \quad (7)$$

where h_0, h_1, \dots, h_n denote the previous user's history embedding trajectory and p represents the probability density function of the data distribution. The proof is included in Appendix C.

Lemma 2 establishes a connection between what is observed and what could potentially occur, enabling us to express the counterfactual probability density with re-weighted empirical samples. Thus we now propose a conditional intensity function $\lambda(\cdot|h)$ and use θ to denote all the parameters in the intensity λ and the history encoder h . We approximate λ_h using re-weighted data according to the lemma, leading to the following learning objective. The proof can be found in Appendix D.

Proposition 1 (Weighted maximum log-likelihood estimation). *Let $\mathcal{D} = \{(x_i^{(k)}, \bar{h}_i^{(k)}, c)\}$ denote the set of observed data tuples, where $x_i^{(k)}$ is the i th observed event of the user k , $\bar{h}_i^{(k)} = (h_0^{(k)}, \dots, h_i^{(k)})$ is the corresponding history embedding trajectory, and c is the user's category. For the sake of clarity, we use the notation of $h(x)$ in place of h to represent the up-to-date history embedding, acknowledging that both terms have been used interchangeably in earlier discussions. The learning objective can be approximated by maximizing the following weighted log-likelihood:*

$$\begin{aligned} \mathbb{E}_h [\mathbb{E}_{x \sim p_h} [\log f(x|h(x))]] &\propto \frac{1}{K} \sum_{(x_i^{(k)}, \bar{h}_i^{(k)}, c) \in \mathcal{D}} w(\bar{h}_i^{(k)}, c) \log f(x_i^{(k)}|h_i^{(k)}), \\ &= \frac{1}{K} \sum_{k=1}^K \left(\int_{\mathcal{X}} w(\bar{h}, c) \log (\lambda(x|h(x))) d\mathbb{N}^{(k)}(x) - \int_{\mathcal{X}} w(\bar{h}_n^{(k)}, c) \lambda(x|h^{(k)}(x)) dx \right) \end{aligned} \quad (8)$$

where K is the number of users, $\mathbb{N}^{(k)}$ is the counting measure for each user indexed by k , respectively. Furthermore, $\bar{h}_n^{(k)}$ denotes the set of observed history embedding for the k th user before $t(x)$. Here w denotes the subject-specific IPTW, which takes the form:

$$w(\bar{h}, c) = \frac{1}{\prod_{i=1}^{n+1} f(h_i|h_{i-1}, c)}. \quad (9)$$

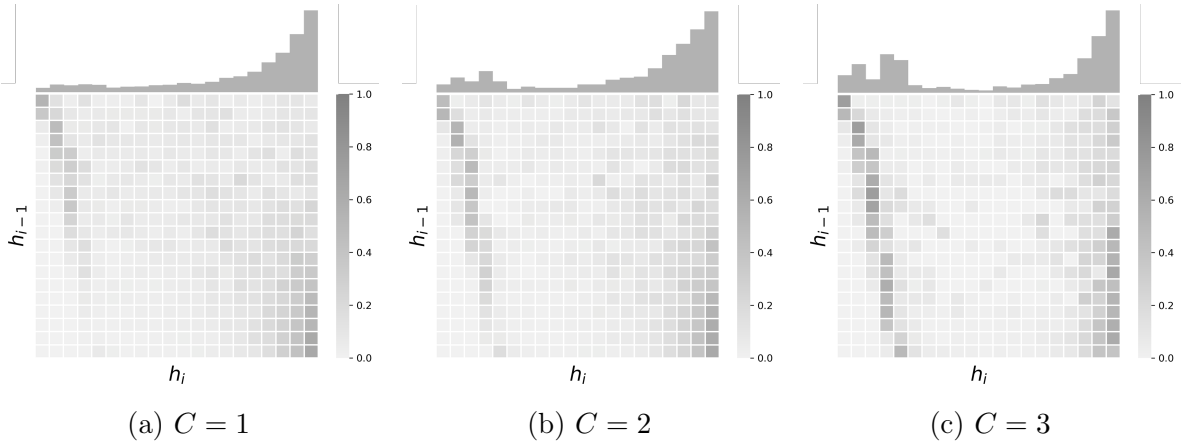


Figure 3: The histogram of $p(h_i|C)$ and the conditional transition probability $p(h_i|h_{i-1}, C)$ for the three categories $C = 1, 2, 3$ when $1/\delta = 20$ visually reveal distinct patterns. These differences in the conditional transition probabilities across user categories highlight their unique behavior pattern.

The proof is included in Appendix D.

Remark 1. *In practice, we can consider using the stabilized weight (SW) instead of the IPTW such that the weights are less prone to exploding due to small denominator values. See [30] for more details.*

$$SW(\bar{h}, c) = \frac{\prod_{i=1}^{n+1} f(h_i|h_{i-1})}{\prod_{i=1}^{n+1} f(h_i|h_{i-1}, c)}.$$

Conditional history transition To learn the model by maximizing (8), one needs to specify the conditional transition probability $f(h_i|h_{i-1}, c)$ between two consecutive history embedding variables h_i and h_{i-1} given the user’s category c . Following [55], we propose a non-parametric binning method to obtain the probability $f(h_i|h_{i-1}, c)$. It comes with three practical benefits: (i) Discretized sample space enables the probability to be discontinuous and identifiable, assisting the positivity assumption; (ii) Bin size can be adjusted to help stabilize weights; (iii) Binning method provides a less complex yet still effective way to estimate probabilities.

Our method is implemented as follows. We partition the unit history embedding space \mathcal{H} uniformly into $1/\delta$ bins of equal size of δ , denoted by $\mathcal{H}_u \in \mathcal{H}$. Without loss of generality, we can treat the category space as a continuous space as well. We can therefore also partition the cluster space \mathcal{C} into R bins of equal size, denoted by \mathcal{C}_r . In this work, however, the cluster space is already discrete. Then the observed conditional history transition space $\Omega := \mathcal{H} \times \mathcal{H} \times \mathcal{C}$ can be constructed as a set of $(1/\delta)^2 \times R$ elements, where each of them can be denoted by $\mathcal{B}(u, u', r) := \mathcal{H}_u \times \mathcal{H}_{u'} \times \mathcal{C}_r \subseteq \Omega$. Here, u and u' are indices of the set \mathcal{H} and r is the index of the set \mathcal{C} . The count of observed conditional history transition tuples in an arbitrary bin \mathcal{B} can be expressed as $\sum_{k=1}^K \sum_{j=1}^{N_T^{(k)}} \mathbb{1}[(h_j^{(k)}, h_{j-1}^{(k)}, c^{(k)}) \in \mathcal{B}(u, u', r)]$, where $\mathbb{1}$ denotes the indicator function.

We can thus obtain a discretized histogram across all bins $\mathcal{B}(u, u', r)$. The probability of an arbitrary tuple (h, h', c') falling in the bin $\mathcal{B}(u, u', r)$ can be approximated by the

proportion of the counts:

$$\widehat{p}(u, u', r) = \frac{\sum_{k=1}^K \sum_{j=1}^{N_T^{(k)}} \mathbb{1}[(h_j^{(k)}, h_{j-1}^{(k)}, c^{(k)}) \in \mathcal{B}(u, u', r)]}{\sum_{k=1}^K N_T^{(k)}}. \quad (10)$$

An example of the conditional transition probabilities and the histograms is visualized in Fig. 3. See Appendix G for more visualization examples. Therefore, the conditional transition probability can be estimated using (10) by

$$\widehat{f}_\delta(h_i|h_{i-1}, c) = \frac{\sum_{(u, u', r)} \widehat{p}(u, u', r) \cdot \mathbb{1}[(h_i, h_{i-1}, c) \in \mathcal{B}(u, u', r)]}{\sum_{u=1}^{1/\delta} \widehat{p}(u, u', r) \cdot \mathbb{1}[h_i \in \mathcal{H}_u]}. \quad (11)$$

With the transition probability estimated, we can approximate the IPTW weights following (9):

$$\widehat{w}_\delta(\bar{h}, c) = \frac{1}{\prod_{i=1}^{n+1} \widehat{f}_\delta(h_i|h_{i-1}, c)}. \quad (12)$$

This method is limited by the dimensionality of the hidden history embedding denoted by q , since the number of bins grows quickly with it. The complexity of obtaining each conditional transition probability scales with q , and that of bin construction scales exponentially.

Sensitivity analysis We now look into how the discretization via binning affects the log-likelihood estimation and then study quantitatively its effects on the history transition probabilities. We denote the true IPTW values calculated based on $f(h_i|h_{i-1}, c)$ as w and define $\ell^*(w)$ as the maximal log-likelihood with optimal model parameters θ^* with the weights w . With discretization over the history embedding space, we denote the weights derived from $\widehat{f}_\delta(h_i|h_{i-1}, c)$ by \widehat{w}_δ . Then $\ell^*(\widehat{w}_\delta)$ refers to the maximal log-likelihood given θ^* when the weights take the value of \widehat{w}_δ .

Proposition 2 (Improvement in binning). *Let the history embedding space \mathcal{H} be uniformly partitioned into bins of equal size δ , we denote the corresponding IPTW derived by \widehat{w}_δ . We have*

$$\ell^*(\widehat{w}_1) \leq \ell^*(\widehat{w}_\delta) \leq \ell^*(w), \quad \forall \delta \in (0, 1].$$

Proof. Following the definition of \widehat{w}_δ in (12), we can see that when $\delta = 1$, the size of the bin is exactly the same as the sample space, with all samples falling into this single bin. Therefore all conditional transition probabilities are 1, *i.e.*, $\widehat{w}_1(\cdot) = 1$. On the other hand, when $\delta < 1$ where there are more than one bins, the conditional probabilities $\widehat{f}_\delta(\cdot) \leq 1$ which leads to $\widehat{w}_\delta \geq 1$. Thus $\ell^*(\widehat{w}_\delta) \geq \ell^*(\widehat{w}_1)$. Additionally, by definition $\ell^*(\widehat{w}_\delta)$ given any δ will be smaller than the true $\ell^*(w)$ whatever the value of δ takes. This leads to $\ell^*(\widehat{w}_\delta) \leq \ell^*(w)$. \square

Remark 2. *This proposition has shown that the introduction of IPTW weights using approximation via discretization in the history embedding space will achieve a non-negative improvement to the log-likelihood function. This indicates the proposed counterfactual framework is guaranteed to improve the performance of the framework when compared to the method without counterfactual weights, regardless of the choice of δ .*

The binning approximation will inevitably introduce bias into the log-likelihood $\ell(\hat{w}_\delta)$ since the weights are approximated in (12). The binning procedure approximates the joint probability $f(h_i, h_{i-1}, c)$ by $\hat{f}_\delta(h_i, h_{i-1}, c)$ as in (11). We analyze the bias and variance introduced by binning following the work of [73].

Lemma 3 (Bias and Variance by binning). *Let history embedding variables h_i and h_{i-1} are of one dimension, which can be extended to higher dimension. Suppose there are m samples of the data tuples (h_i, h_{i-1}, c) , and our objective is to estimate the true joint probability function $f(h_i, h_{i-1}, c)$ (shorthanded by f) utilizing the binning approximation. Denoting the bin size by δ , then the bias and variance of the estimator \hat{f}_δ are as follows:*

$$\begin{aligned} \text{Bias}[\hat{f}_\delta] &= \left(\frac{1}{2} \frac{\partial f}{\partial h_i} + \frac{1}{2} \frac{\partial f}{\partial h_{i-1}} \right) \delta + \mathcal{O}(\delta^2) + \mathcal{C} \\ \text{Var}[\hat{f}_\delta] &= \frac{f}{m\delta^2} + \mathcal{O}\left(\frac{1}{m}\right), \end{aligned}$$

where \mathcal{C} is a constant not dependent on δ or m . Since δ is presumed to be small, higher order terms denoted by $\mathcal{O}(\delta^2)$ are deemed negligible. See Appendix E for detailed derivations.

Remark 3. *From the lemma, we observe the bias of estimator increases with the bin size δ , suggesting coarser bins lead to less accurate estimate. The variance shows it increases as δ decreases. This reflects a trade-off between bias and variance, as smaller bin size makes the bias smaller but will increase the variance in the estimator. Additionally, the variance decreases as m increases, which suggests more data tuples will reduce the variance, as expected.*

The bias and the variance of the estimator \hat{f} constructed by binning provide a way to obtain the optimal bin size by minimizing the integrated mean square error (IMSE) which is formulated as

$$\text{IMSE}(\delta) = \int \int (\text{Bias}^2 + \text{Var}) dh_i dh_{i-1} \quad (13)$$

Here we assume that when the number of events gets sufficiently large in a sequence, the relationship between events stabilizes and the joint probability function $f(h_i, h_{i-1}, c)$ becomes symmetrical between h_i and h_{i-1} . This enables the simplification of the partial derivatives which we denote by f' :

$$\frac{\partial f}{\partial h_i} = \frac{\partial f}{\partial h_{i-1}} = f'.$$

Proposition 3 (Optimal bin size). *Following the same assumptions by Lemma 3 and the aforementioned symmetry assumption of partial derivatives, the optimal bin size can be obtained by minimizing the IMSE between the true probability density function f and the estimator by binning \hat{f} . When $\int f' \neq 0$, the optimal bin size is as follows:*

$$\delta^* = \left(\frac{2}{(\int f')^2} \right)^{1/4} m^{-1/4}.$$

When $\int f' = 0$, the optimal bin size is as follows:

$$\delta^* = \left(\frac{4}{\int f'^2} \right)^{1/5} m^{-1/5}.$$

The proof is detailed in Appendix F.

Remark 4. Proposition 3 indicates the asymptotically optimal choice of bin size depends on both the partial derivative f' and the number of samples m . A larger m pushes the optimal choice of δ smaller. For example, a ten-fold increase in sample numbers m will shrink δ^* by a factor of 0.56. It also depends on the probability density function f as well. If f is a bivariate normal distribution with zero mean $\mu = 0$, isotropic deviation $\sigma = 1$, and correlation coefficient ρ , the approximated $\delta^* \approx (24\pi^2(1-\rho)(1+\rho)^3/m)^{1/5}$. For detailed proof refer to the appendix.

4.2 Alternate learning algorithm

We learn the model parameters θ of the counterfactual intensity by optimizing the weighted log-likelihood function in (8). We note that the IPTW values $w(\bar{h}, c)$ need to be obtained separately, because they rely on the conditional transition probabilities $f(h_i|h_{i-1}, c)$ which are calculated apart from the model parameters via (9). They change as training progresses. It indicates there is *cyclic dependence* between the weights $w(\bar{h}, c)$ and the model parameters. Therefore, to obtain estimates for both θ and $w(\bar{h}, c)$, it is necessary to conduct an alternate optimization.

Calculating the objective function in (8) requires more attention. The first integral can be directly computed, while the second integral can only be approximated. We utilize a Monte Carlo sampling scheme to approximate the second integral. In this work, the event space $\mathcal{X} = [0, T) \times \mathcal{M}$ is constructed on the continuous temporal space and the discrete mark space, so we need only to draw samples from the temporal space. Denote the set of samples randomly drawn from the temporal space by $t \in \mathcal{T}$ and the set of random samples in the mark space by $m \in \mathcal{M}$, then we have

$$\int_{\mathcal{X}} w(\bar{h}_n^{(k)}, c) \lambda_{\theta}(x|h^{(k)}(x)) dx \approx \frac{T}{|\mathcal{M}| \cdot |\mathcal{T}|} \sum_{t \in \mathcal{T}} \sum_{m \in \mathcal{M}} w(\bar{h}_n^{(k)}, c) \lambda_{\theta}(t, m|h^{(k)}). \quad (14)$$

Given the objective log-likelihood function (8) and the IPTW expression (12), we propose a joint learning algorithm to obtain estimates for both the model parameters $\hat{\theta}$ and the IPTW values \hat{w}_{δ} in Algorithm 1 with details on implementation.

4.3 Inference for prediction

The prediction and inference of the proposed model follow the standard point processes inference method [82]. To be specific, the predictions are obtained given the past event sequences of new users without their category information. To carry out inference, we need to obtain the counterfactual intensity $\lambda_h(x)$, which is approximated by the conditional intensity function $\lambda_{\theta}(x|h)$. We then proceed to obtain the probability density function from the conditional intensity following (2):

$$f_{\theta}(x|h) = \lambda_{\theta}(x|h) \cdot \exp \left(- \int_{[t_n, t(x)) \times \mathcal{M}} \lambda_{\theta}(u|h) du \right). \quad (15)$$

Algorithm 1: Counterfactual intensity learning

Data: Event sequences of K users: $\mathcal{D} = \{x^{(1)}, x^{(2)}, \dots, x^{(K)}\}$;
 Number of events of K users: $N_T^{(1)}, N_T^{(2)}, \dots, N_T^{(K)}$;
 Category of K users: $c^{(1)}, c^{(2)}, \dots, c^{(K)}$.

1 **Parameters:** Number of training epochs: E ; Number of batches: B ;
 2 Hyperparameters: δ, η .
 3 **Initialization:** IPTW values $w_\delta(\bar{h}, c) = 1, \forall \bar{h}, c$.
 4 **for** $e = 1 : E$ **do**
 5 $\mathcal{G} \leftarrow \emptyset, \mathcal{F} \leftarrow \emptyset$;
 6 **for** $b = 1 : B$ **do**
 7 Randomly select κ user event sequences $\mathcal{D}_b := \{x^{(k)}\} \subset \mathcal{D}$;
 8 **for** $k = 1 : \kappa$ **do**
 9 **for** $i = 1 : N_T^{(k)}$ **do**
 10 $h_i^{(k)} \leftarrow \phi(x_i^{(k)}, h_{i-1}^{(k)})$ for all $x_i \in x^{(k)}$ via (4);
 11 $\mathcal{G} \leftarrow \mathcal{G} \cup \{(h_i^{(k)}, h_{i-1}^{(k)}, c^{(k)})\}$;
 12 $\bar{h}_i^{(k)} \leftarrow (h_0^{(k)}, \dots, h_i^{(k)})$;
 13 $\mathcal{F} \leftarrow \mathcal{F} \cup \{(x_i^{(k)}, \bar{h}_i^{(k)}, c^{(k)})\}$;
 14 $S \leftarrow 0$;
 15 **for** $(x_i^{(k)}, \bar{h}_i^{(k)}, c^{(k)})$ in \mathcal{F} **do**
 16 Obtain $f(x_i^{(k)} | h_i^{(k)})$ from $\lambda(x_i^{(k)} | h^{(k)}(x))$ via (2) & (5);
 17 $S \leftarrow S + w_\delta(\bar{h}_i^{(k)}, c^{(k)}) \log f(x_i^{(k)} | h^{(k)}(x))$;
 18 $\theta \leftarrow \arg \max_\theta S$ in (8);
 19 **if** $e // \eta = 0$ **then**
 20 $\mathcal{L} \leftarrow \{(u, v, r) | 1 \leq u, v \leq 1/\delta, 1 \leq R, u, v, r \in \mathbb{Z}\}$;
 21 **for** $(u, v, r) \in \mathcal{L}$ **do**
 22 $p(u, v, r) \leftarrow \frac{\sum_{\mathcal{G}} \mathbb{1}[(h_i^{(k)}, h_{i-1}^{(k)}, c^{(k)}) \in \mathcal{B}(u, v, r)]}{\sum_{k=1}^K N_T^{(k)}}$ via (10);
 23 **for** $(u, v, r) \in \mathcal{L}$ **do**
 24 $f_\delta(\frac{u-1}{\delta} \leq h_i < \frac{u}{\delta} | \frac{v-1}{\delta} \leq h_{i-1} < \frac{v}{\delta}, c = r) \leftarrow \frac{p(u, v, r)}{\sum_u p(u, v, r)}$ in (11);
 25 **for** $k = 1 : K$ **do**
 26 **for** $i = 1 : N_T^{(k)}$ **do**
 27 $\bar{h}_i^{(k)} \leftarrow (h_0^{(k)}, \dots, h_i^{(k)})$;
 28 $w_\delta(\bar{h}_i^{(k)}, c^{(k)}) \leftarrow 1 / \prod_{i'=1}^i f_\delta(h_{i'}^{(k)} | h_{i'-1}^{(k)}, c^{(k)})$ via (12);
Result: Optimal IPTW values $\hat{w}_\delta(\bar{h}, c)$; Optimal model parameters $\hat{\theta}$.

Subsequently, the prediction for both the next upcoming event $\hat{x} = (\hat{t}, \hat{m})$ can be analytically calculated from (15):

$$\hat{x} = \int_{[t_n, t(x)) \times \mathcal{M}} x f_\theta(x | h) dx. \quad (16)$$

When the mark variable m is discrete, (16) can be further split to time and mark predictions separately as follows:

$$\begin{aligned}\hat{t} &= \int_{t_n}^{\infty} \tau \sum_{m \in \mathcal{M}} f_{\theta}(\tau, m|h) d\tau, \\ \hat{m} &= \arg \max_{m \in \mathcal{M}} \int_{t_n}^{\infty} f_{\theta}(\tau, m|h) d\tau.\end{aligned}\tag{17}$$

The integrals in (15), (16), and (17) can be estimated via discretization of the domain. In addition to direct calculation, one can also elect to draw multiple samples via simulation and then take the average to obtain the event prediction. It is typically conducted by using the thinning algorithm [58], which offer more insight on uncertainty of the temporal prediction. See [64] for more details regarding prediction and thinning.

5 Experiments

To evaluate the efficacy of the proposed counterfactual event prediction framework, we apply it in several simulation studies and to two real-world applications. We compare the performance of the proposed framework in these studies against several popular point processes as baseline models.

5.1 Synthetic studies

In the simulation studies, we first investigate the performance of the proposed framework in a range of scenarios mimicking what typically takes place in reality. This part of the study ensures the proposed method is capable of accommodating common situations. We also carry out an ablation study of the framework looking into how the model's hyper-parameters can impact the performance in event prediction.

Experimental setup Throughout the simulation study, we obtain training data and testing data by generating them from known point process models. Both the training and the testing data sequences are generated from $|\mathcal{C}| = 3$ clusters each corresponding to a different point process model or a set of similar models. The events are confined in the time domain of $[0, T)$, where $T = 100$. For example, sequences from each cluster can be sampled from a distinct point process model such that the user behavior between clusters is different. For the testing set, the cluster information for the sequences is taken out. We obtain a total of 1,200 sequences for the training set, and an additional 300 for the testing set. We conduct multiple experiments to account for various scenarios corresponding to potential use cases in the real world. Across the experiments, we evaluate the proposed framework against a set of baseline methods on its prediction performance. Additionally, we carry out an ablation study to investigate the effects of parameters of our model on its performance.

Baselines: We elect to utilize four point process models commonly utilized in event sequence data modeling, including Neural Hawkes (NH) method, Recurrent Marked Temporal Point Process (RMTPP) model, temporal Hawkes process with exponential triggering function (Exp Hawkes), and self-correcting point process (Self-corr). The

baseline methods cover a wide range of different approaches to point process modeling from the basic Hawkes model to the state-of-the-art ones utilizing hidden embedding variables including NH and RMTPP. For our counterfactual framework, we apply the weighting scheme to construct Counterfactual-Neural Hawkes (C-NH) and Counterfactual-RMTPP (C-RMTPP) such that we can directly evaluate the performance between NH and C-NH and for RMTPP as well. Additionally, the self-correcting point process is included given its different triggering structure and serves as an additional reference in baseline.

Evaluation metrics: We elect to utilize the mean absolute error (MAE) of the predicted conditional intensity as the error metric in the testing set. Since in this study the conditional intensity functions for the sequence-generating models are specified and known, we directly compare the true conditional intensity against the estimate with parameters fitted by each method. For each event sequence in the testing set, we calculate the mean of the difference between the true conditional intensity function and the estimated intensity function across the time domain, arriving at the MAE value.

Synthetic data: We investigate a number of synthetic experiments in this study, which we briefly introduce as follows. For more details please refer to the appendix:

1. Three categories each generate 400 event sequences for the training set, and an additional 100 for the testing one. Sequences within the same category is generated by a temporal Hawkes point process model with exponential triggering function and parameters fixed. Hidden embedding dimension is set to $q = 1$ and the number of bins $1/\delta = 25$, number of epochs $\eta = 5$.
2. We keep the same setting for the Hawkes models of the three categories, but composition of event sequences from each category is no longer balanced. There are now 200 sequences generated by the first Hawkes model, 400 by the second, and 600 by the third one, thereby creating an unbalanced dataset between three categories.
3. Composition is further changed. Now 600 sequences are now generated by the first Hawkes model, 400 by the second, and 200 by the third one. This is another unbalanced training set.
4. Three Hawkes processes for the three categories with parameters no longer fixed. The 1,200 sequences are evenly divided between categories, but the parameter values are drawn from fixed random variables when sampling for each sequence. Event sequences in each category observe a different yet still similar behavior.
5. We utilize different families of point process models for the three categories. For the first and the second categories, we still utilize two exponential Hawkes process with different parameter. For the third category, we elect to use a Neural Hawkes model. Each category still contributes 400 training and 100 testing sequences.
6. We look into more complex event data with an additional mark variable, *i.e.* the marked point process. We append an additional discrete mark variable to the event sequences generated. We utilize three marked-temporal Hawkes processes for simulation, each contributing the same number of sequences.

Table 1: Prediction MAE of synthetic experiments.

Syn Exp No.	R-NH	NH	C-NH	R-RMPTT	RMTPP	C-RMPTPP	Exp Hawkes	Self-Corr
1	1.6545	1.0308	0.9145	2.5738	1.9304	1.8751	2.8332	2.6224
2	1.5544	1.0019	0.9611	2.2110	1.7429	1.7010	1.5854	2.3097
3	1.6760	0.9217	0.9055	2.2965	1.8711	1.8128	1.2508	1.9449
4	1.4612	1.2222	0.9986	2.0820	1.5833	1.5542	1.4748	1.8293
5	2.0417	1.4299	1.4067	2.4207	2.0234	1.9868	2.1177	2.7442
6	2.5801	1.0796	1.0523	2.3872	1.9197	1.8127	n/a	n/a

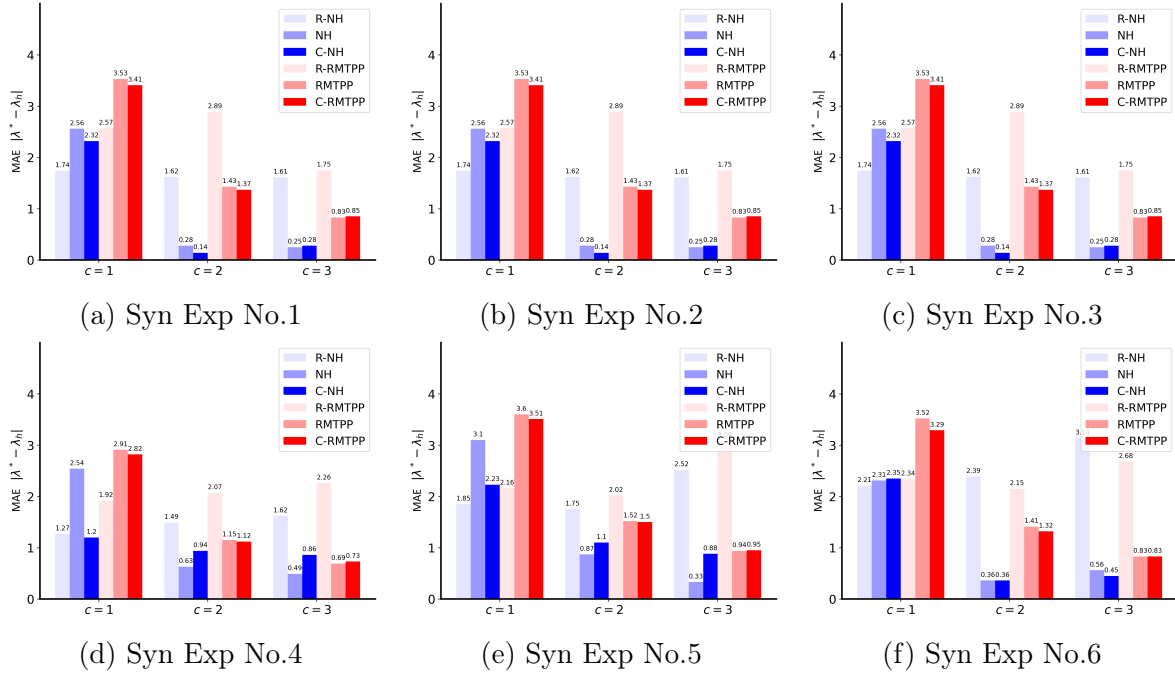
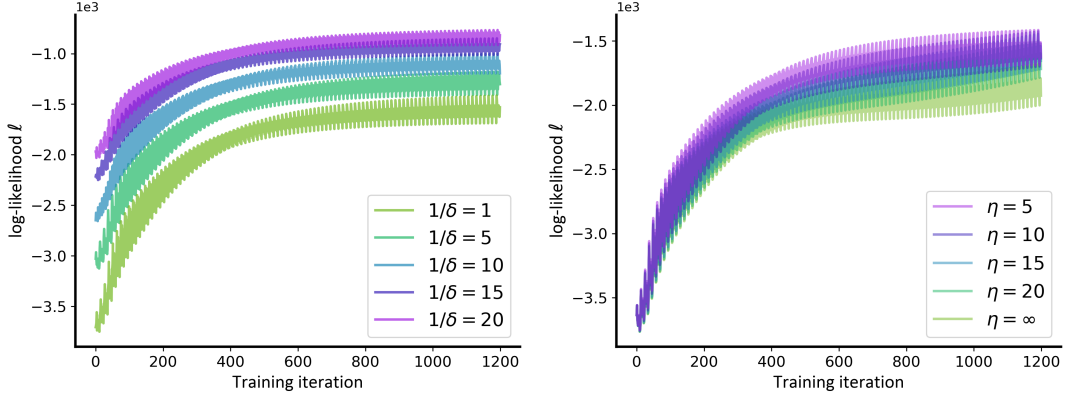


Figure 4: Category-wise prediction MAE of synthetic experiments.

Results For the six synthetic experiments, we carry out the prediction and calculate the errors with results shown in Table 1. For a more detailed breakdown on MAE values across different categories in the testing set, the results are illustrated in Fig. 4. From the numerical results, we can observe that the performance by C-NH and C-RMPTP are in general better than their counterparts without the reweighting scheme. Although the counterfactual framework generally works better overall, there are cases where it underperforms its counterpart on the prediction MAE for individual categories.

From Synthetic Exp. 1-3, we can see that C-NH retains a smaller MAE values when compared to NH, usually by 5-10% even at different composition settings between categories. For C-RMPTP it outperforms RMTPP by approx. 3% as well. The two counterfactual methods perform better than the two other baseline methods as well. For Exp. 4, we are seeing a similar behavior where the counterfactual framework reduces the MAE values by roughly 10%, suggesting our framework works even better with more complicated user behavior within the same cluster. The same goes with Exp. 5, which validates the observation. For these two experiments, the performance of Exp Hawkes gets better than RMTPP but NH remains the best. This could partly due to the fact that the event sequences are generated from Hawkes process models with exponential



(a) The number of bins $1/\delta$.

(b) The number of epochs η .

Figure 5: Log-likelihood convergence analysis.

triggering functions in the first place, and therefore easier for Exp Hawkes to fit. For the final experiment with marks, we observe a 2-4% reduction in MAE values for the proposed counterfactual methods over the baselines as well.

Additionally, we analyze the MAE values for each category in the synthetic experiments as well from Fig. 4. The prediction errors for sequences from the first category with the most events are usually higher than the other two, regardless of the method. Additionally, we observe that the proposed counterfactual methods generally achieves an improvement in terms of prediction errors for user sequences from all three categories. There are two exceptions to it, including the errors for sequences from the third category by C-RMTPP in Exp. 1-3 compared to RMTPP, and the ones for sequences from the second and the third categories by C-NH in Exp. 4&5 compared to NH. As a side note, R-NH and R-RMTPP produce roughly the same MAE values across the three categories, which is expected given the random category assignment.

Hyper-parameter selection Beyond the synthetic studies, we now look more closely into the hyper-parameters of the counterfactual framework and how they affect the performance of the method in prediction. Our proposed framework utilizes two parameters that can be tuned: (i) the number of bins used to approximate the conditional transition probability, denoted by $1/\delta$, and (ii) the number of epochs at which pace the IPTW weights are updated, denoted by η . In short, η inversely reflects the frequency of re-fitting the conditional transition probabilities. In this ablation study, we investigate how these two model parameters influence the prediction performance of the model.

We generate 1,200 training sequences and 300 testing sequences from three Hawkes process models with fixed parameters evenly such that each category contributes 400 training and 100 testing sequences. This is the same setting as Synthetic experiment 1. We compare the two counterfactual methods C-NH and C-RMTPP with their counterparts NH and RMTPP. We fix the dimension of embedding $p = 1$ while the other model parameters change, and evaluate them using the error metric MAE. Additionally, we plot the change of training log-likelihood ℓ over 100 training iterations to study the convergence behavior.

Number of bins $1/\delta$: In this study, we study the effect on the proposed method when we alter the number of bins used to approximate conditional history transition probabilities. We fix the number of epochs $\eta = 5$ and vary δ to take several different

Table 2: MAE *w.r.t.* the number of bins $1/\delta$.

# bins ($1/\delta$)	C-NH	Pct.	C-RMTPP	Pct.
1*	1.0155	0%	1.6559	0%
5	0.9347	-8.0%	1.5442	-6.7%
10	0.9145	-10.0%	1.5029	-9.2%
15	0.9066	-10.7%	1.4788	-10.6%
20	0.9012	-11.3%	1.4691	-11.3%

* $1/\delta = 1$ leads to no discretization and all weights taking the value of 1, reverting the method to its unweighted version.

 Table 3: MAE *w.r.t.* the number of epochs η .

# epochs (η)	C-NH	Pct.	C-RMTPP	Pct.
5	0.9388	-7.5%	1.5570	-6.0%
10	0.9455	-6.9%	1.5630	-5.6%
15	0.9560	-5.9%	1.5833	-4.4%
20	0.9683	-4.6%	1.5995	3.4%
∞^*	1.0155	0%	1.6559	0%

* $\eta = \infty$ leads to no update of IPTW weights throughout the training procedure, with all weights staying at 1, reverting the method to its unweighted version.

values. We also include the extreme case when $\delta = 1$, which corresponds to no discretization takes place and all weights remain at 1, *i.e.* becoming the unweighted baselines. The results are shown in Table 2 and the convergence behavior is plotted in Fig. 5(a). We observe that as $1/\delta$ increases the prediction MAE values for both C-NH and C-RMTPP decrease consistently. However, the decrease for both methods is slow and relatively insignificant. It can be deducted that making the discretization finer when approximating the conditional transition probabilities is able to improve prediction performance. On the other hand, there is a trade-off between the improvement in error metric and the additional computational cost when $1/\delta$ gets larger.

Number of epochs η : In this study, we look into the effect on the model when we alter the number of epochs η at which pace the IPTW weights are fitted. We fix the number of bins to $1/\delta = 10$ and vary η to construct several test cases. We include the extreme case when $\eta = \infty$, which corresponds to when the IPTW weights are never updated after being initialized to 1. This is effectively the unweighted case. The results are shown in Table 3 and the convergence behavior is plotted in Fig. 5(b). We observe as η gets smaller the MAE for both methods decrease. This is reasonable since a lower frequency of updating the IPTW weights is expected to lead to worse prediction performance. However, compared to the δ study, the relative change in MAE for this η study is smaller. It suggests the model does not necessarily require a very small η to remain effective and we can save some computation by tuning η accordingly. The convergence plot indicates the convergence behavior is not severely affected either.

5.2 Real case studies

In the real case studies, we evaluate two applications: Netflix user rating prediction and Amazon seller contact prediction. The case studies deal with event sequence data with an additional discrete mark variable describing the type of events. We utilize the same four baseline methods as the synthetic experiments, and the two proposed counterfactual methods **C-NH** and **C-RMTPP**.

Evaluation metrics: Since in the real case studies, the true conditional intensity is no longer available, we now utilize different error metrics for performance evaluation and comparison. For time prediction, we calculate the error between the predicted time and the actual time of occurrence for the next event. We then calculate the mean absolute error (MAE) across all testing event sequences. For mark prediction, we calculate the accuracy of the top five predicted marks against the actual mark for the next event, abbreviated by Acc. In other words, we look for the proportion of predictions in the testing sequences where the top five guesses by the methods cover the true mark of the upcoming event.

Netflix ratings The Netflix ratings data is a public dataset that records the user ratings on movies [5]. The data for each anonymous user include the date they rated a movie and the rating (from 1 to 5) the user provided for the corresponding movie. We import the movie genre information to each movie from the public website IMDB.com, and look for positive ratings (3 to 5) from the users. This way each movie rating event for a single user is now characterized by time and the movie genre is denoted as a tuple (t, m) where the genre is taken up as the mark variable. We therefore treat the rating records for each user as an event sequence. Furthermore, we divide the Netflix users into different categories based on their respective favorite movie genres given the ratings provided by them. We aim to predict the time and movie genre of the next rating event for "new" users not yet observed in the rating history data.

We take 50,000 entries by 300 Netflix users from the entire dataset to form the training dataset. The training set contains 300 user sequences scaled to a time frame of $[0, T)$ with $T = 100$, containing movies from 45 genres. After pre-processing, the selected dataset contains 6712 discrete events from these 300 users over three years, then scaled to a time frame of $[0, T)$ with $T = 100$. We fix the number of movie genres to be investigated to 45. In other words, the categorical mark has 45 potential values. These 300 users are divided into ten different categories by the most-preferred movie genre they rate positively. For prediction, we further obtain the rating event sequences of 75 additional "new" users without obtaining their category information due to their lack of clear preference towards a certain genre. We set the dimension of the hidden embedding variable to $q = 3$ and the number of bins $1/\delta = 125$. Additionally, we set $\eta = 5$.

For evaluation, since the true conditional intensity is no longer available, we now utilize different error metrics for performance comparison. For time prediction, we propose to calculate the MAE between the predicted time of the next event and the actual time for the testing event sequences. For mark prediction, we propose to calculate the accuracy of the top 5 predicted marks against the actual mark for the next event given the large number of potential mark values, abbreviated by Acc. In other words, the proportion of prediction cases where the top 5 guesses cover the true mark value of the upcoming event. Note the exponential Hawkes model and the self-correcting model

Table 4: Numerical Results for real case studies.

Real Exp	Metric	R-NH	NH	C-NH	R-RMTPP	RMTPP	C-RMTPP
Netflix	MAE	6.2633	5.6598	5.6323	6.3853	5.6529	5.6278
	Acc. ¹	0.160	0.293	0.307	0.147	0.267	0.347
Amazon	MAE	14.3511	4.3830	4.2291	4.2643	4.2526	4.1690
	Acc. ¹	0.172	0.238	0.274	0.138	0.190	0.226

¹ Acc. refers to the accuracy predicting the actual discrete intent on whether it is included in the five most likely intents predicted by each method.

are not capable of handling the mark variable, so they are excluded in this case.

The results are shown in Table 4. They indicate the performance of our proposed methods is better than the baselines both in terms of time prediction and mark prediction. For time prediction, the proposed methods achieve a 0.5% improvement over their counterparts, partly due to the smaller size of the dataset. For mark accuracy, the improvement is larger at 5% and 30% for C-NH and C-RMTPP respectively. The random baselines are worse than the others.

Amazon seller contact Finally, we investigate the Amazon seller contact intent prediction problem which motivates our work. The seller support contact dataset from Amazon presented in this work includes user contact events from thousands of sellers sampled from recent years [16]. For each contact event, we have the information on the corresponding anonymous user ID, the time of the contact, and the identified contact intent marked by support associates. We regard the discrete intent as the mark variable, which can take any of the 117 possible values. Additionally, for data privacy purposes, the user identity is anonymized, and the contact time is polluted lightly with random noise.

We obtain from the data 3,000 user event sequences, where each sequence records the contact of an Amazon seller. Each event contains the time of the contact event and a discrete mark variable for the corresponding intent. The 3,000 users for training fall into 12 categories, and we further obtain 500 user event sequences without category information for testing. Our objective in this application is to predict the next contact time and intent for these 500 users in the testing dataset. For the counterfactual framework, we set $q = 3$, the update period $\eta = 5$, and the bin number to $1/\delta = 125$. The results are shown in Table 4 as well.

From the results, we observe our proposed methods perform better as well. For time prediction, the MAE is lower by 4% and 2% respectively for C-NH and C-RMTPP. The mark accuracy is higher by 15% and 19% as well.

6 Conclusions

In this work, we investigated the user-event prediction problem, where we aim to conduct event prediction for new users without category information. We addressed the challenge of unbiased prediction for "new" users through the proposed counterfactual framework reweighting data by IPTW. It is evaluated using a series of simulation studies and two real-world cases, which demonstrate improvement in prediction performance. We

validated the efficacy of our proposed framework using a series of simulation studies, which shows the reweighting scheme improves the prediction performance of point process models consistently utilizing hidden history variables. This work has shown that by introducing the weights from conditional transition probabilities, bias can be reduced in the prominent point process models that encode historical information using a set of hidden variables.

There are two limitations of this work. So far we have only been applying the framework to hidden variables of relatively lower dimension due to computational constraints, but oftentimes they need to be high dimensional as well. Additionally, the sensitivity analysis performed on the binning procedure for conditional transition probabilities relies on relatively strong assumptions which may be impractical in application.

Going forward, we aim to update the IPTW values more efficiently, for example, establishing a different approach to estimating the conditional probabilities without having to rely on the discrete binning method. This will significantly improve the computational efficiency.

References

- [1] Hyung Jun Ahn. A new similarity measure for collaborative filtering to alleviate the new user cold-starting problem. *Information Sciences*, 178(1):37–51, 2008.
- [2] Ahmed Alaa and Mihaela Van Der Schaar. Validating causal inference models via influence functions. In *International Conference on Machine Learning*, pages 191–201. PMLR, 2019.
- [3] Ahmed M Alaa and Mihaela Van Der Schaar. Bayesian inference of individualized treatment effects using multi-task Gaussian processes. *Advances in neural information processing systems*, 30, 2017.
- [4] Ahmed M Alaa and Mihaela van der Schaar. Bayesian nonparametric causal inference: Information rates and learning algorithms. *IEEE Journal of Selected Topics in Signal Processing*, 12(5):1031–1046, 2018.
- [5] James Bennett, Stan Lanning, et al. The Netflix prize. In *Proceedings of KDD Cup and Workshop*, volume 2007, page 35. New York, 2007.
- [6] Patrik Berger and Michal Kompan. User modeling for churn prediction in E-commerce. *IEEE Intelligent Systems*, 34(2):44–52, 2019.
- [7] Ioana Bica, James Jordon, and Mihaela van der Schaar. Estimating the effects of continuous-valued interventions using generative adversarial networks. *Advances in Neural Information Processing Systems*, 33:16434–16445, 2020.
- [8] Jesús Bobadilla, Fernando Ortega, Antonio Hernando, and Jesús Bernal. A collaborative filtering approach to mitigate the new user cold start problem. *Knowledge-based Systems*, 26:225–238, 2012.
- [9] Moira Burke, Cameron Marlow, and Thomas Lento. Feed me: Motivating newcomer contribution in social network sites. In *Proceedings of the SIGCHI conference on human factors in computing systems*, pages 945–954, 2009.

- [10] David F. Carr. Threads app usage down 79 2023.
- [11] Yehu Chen, Annamaria Prati, Jacob Montgomery, and Roman Garnett. A multi-task Gaussian process model for inferring time-varying treatment effects in panel data. In *International Conference on Artificial Intelligence and Statistics*, pages 4068–4088. PMLR, 2023.
- [12] Dawei Cheng, Sheng Xiang, Chencheng Shang, Yiyi Zhang, Fangzhou Yang, and Liqing Zhang. Spatio-temporal attention-based neural network for credit card fraud detection. In *Proceedings of the AAAI conference on artificial intelligence*, volume 34, pages 362–369, 2020.
- [13] Wen-Hao Chiang, Xueying Liu, and George Mohler. Hawkes process modeling of COVID-19 with mobility leading indicators and spatial covariates. *International Journal of Forecasting*, 38(2):505–520, 2022.
- [14] Daryl J Daley, David Vere-Jones, et al. *An Introduction to the Theory of Point Processes: Volume I: Elementary Theory and Methods*. Springer, 2003.
- [15] Li Dong, Matthew C Spencer, and Amir Biagi. A semi-supervised multi-task learning approach to classify customer contact intents. In *Proceedings of the 4th Workshop on e-Commerce and NLP*, pages 49–57, 2021.
- [16] Matthew C. Dong, Li; Spencer. Amazon seller contact intent sequence dataset. 2023.
- [17] Nan Du, Hanjun Dai, Rakshit Trivedi, Utkarsh Upadhyay, Manuel Gomez-Rodriguez, and Le Song. Recurrent marked temporal point processes: Embedding event history to vector. In *Proceedings of the 22nd ACM SIGKDD International Conference on Knowledge Discovery and Data Mining*, pages 1555–1564, 2016.
- [18] Nan Du, Yichen Wang, Niao He, Jimeng Sun, and Le Song. Time-sensitive recommendation from recurrent user activities. *Advances in Neural Information Processing Systems*, 28, 2015.
- [19] eBay Inc. eBay Inc. reports fourth quarter and full year 2023 results, 2023.
- [20] Michelle Faverio. Majority of us twitter users say they've taken a break from the platform in the past year. 2023.
- [21] Ignacio Fernández-Tobías, Matthias Braunhofer, Mehdi Elahi, Francesco Ricci, and Iván Cantador. Alleviating the new user problem in collaborative filtering by exploiting personality information. *User Modeling and User-Adapted Interaction*, 26:221–255, 2016.
- [22] Garrett Fitzmaurice, Marie Davidian, Geert Verbeke, and Geert Molenberghs. *Longitudinal Data Analysis*. CRC Press, 2008.
- [23] Vreixo Formoso, Diego Fernández, Fidel Cacheda, and Victor Carneiro. Using profile expansion techniques to alleviate the new user problem. *Information processing & management*, 49(3):659–672, 2013.

- [24] Eric W Fox, Martin B Short, Frederic P Schoenberg, Kathryn D Coronges, and Andrea L Bertozzi. Modeling e-mail networks and inferring leadership using self-exciting point processes. *Journal of the American Statistical Association*, 111(514):564–584, 2016.
- [25] Michele Garetto, Emilio Leonardi, and Giovanni Luca Torrisi. A time-modulated hawkes process to model the spread of COVID-19 and the impact of countermeasures. *Annual Reviews in Control*, 51:551–563, 2021.
- [26] Yingqiang Ge, Shuchang Liu, Ruoyuan Gao, Yikun Xian, Yunqi Li, Xiangyu Zhao, Changhua Pei, Fei Sun, Junfeng Ge, Wenwu Ou, et al. Towards long-term fairness in recommendation. In *Proceedings of the 14th ACM International Conference on Web Search and Data Mining*, pages 445–453, 2021.
- [27] Alex Graves and Alex Graves. *Supervised Sequence Labelling*. Springer, 2012.
- [28] Moritz Hardt, Eric Price, and Nati Srebro. Equality of opportunity in supervised learning. *Advances in Neural Information Processing Systems*, 29, 2016.
- [29] Alan G Hawkes. Spectra of some self-exciting and mutually exciting point processes. *Biometrika*, 58(1):83–90, 1971.
- [30] Miguel A Hernán and James M Robins. *Causal Inference*. CRC, 2010.
- [31] Jose Antonio Iglesias, Plamen Angelov, Agapito Ledezma, and Araceli Sanchis. Creating evolving user behavior profiles automatically. *IEEE transactions on knowledge and data engineering*, 24(5):854–867, 2011.
- [32] Kosuke Imai and David A Van Dyk. Causal inference with general treatment regimes: Generalizing the propensity score. *Journal of the American Statistical Association*, 99(467):854–866, 2004.
- [33] Meta Platforms Inc. Meta reports third quarter 2023 results, 2023.
- [34] Snap Inc. Snap Inc. 2023 investor day - recap, 2023.
- [35] Milan Janić. Modeling the large scale disruptions of an airline network. *Journal of transportation engineering*, 131(4):249–260, 2005.
- [36] Dazhi Jiang, Zhichao Liu, Lin Zheng, and Jianwei Chen. Factorization meets neural networks: A scalable and efficient recommender for solving the new user problem. *IEEE Access*, 8:18350–18361, 2020.
- [37] Johannes Jurgovsky, Michael Granitzer, Konstantin Ziegler, Sylvie Calabretto, Pierre-Edouard Portier, Liyun He-Guelton, and Olivier Caelen. Sequence classification for credit-card fraud detection. *Expert systems with applications*, 100:234–245, 2018.
- [38] Bill Karakostas. Event prediction in an IoT environment using naïve Bayesian models. *Procedia computer science*, 83:11–17, 2016.

- [39] Edward H Kennedy, Zongming Ma, Matthew D McHugh, and Dylan S Small. Non-parametric methods for doubly robust estimation of continuous treatment effects. *Journal of the Royal Statistical Society Series B: Statistical Methodology*, 79(4):1229–1245, 2017.
- [40] Daniel Kluver and Joseph A Konstan. Evaluating recommender behavior for new users. In *Proceedings of the 8th ACM Conference on Recommender Systems*, pages 121–128, 2014.
- [41] Che-Yu Kuo and Jen-Tzung Chien. Markov recurrent neural networks. In *2018 IEEE 28th International Workshop on Machine Learning for Signal Processing (MLSP)*, pages 1–6. IEEE, 2018.
- [42] Matt J Kusner, Joshua Loftus, Chris Russell, and Ricardo Silva. Counterfactual fairness. *Advances in Neural Information Processing Systems*, 30, 2017.
- [43] Trent Kyono, Yao Zhang, Alexis Bellot, and Mihaela van der Schaar. MIRACLE: Causally-aware imputation via learning missing data mechanisms. *Advances in Neural Information Processing Systems*, 34:23806–23817, 2021.
- [44] Günter Last and Mathew Penrose. *Lectures on the Poisson process*, volume 7. Cambridge University Press, 2017.
- [45] Rui Li, Stephanie Hu, Mingyu Lu, Yuria Utsumi, Prithwish Chakraborty, Daby M Sow, Piyush Madan, Jun Li, Mohamed Ghalwash, Zach Shahn, et al. G-Net: A recurrent network approach to g-computation for counterfactual prediction under a dynamic treatment regime. In *Machine Learning for Health*, pages 282–299. PMLR, 2021.
- [46] Shuang Li, Shuai Xiao, Shixiang Zhu, Nan Du, Yao Xie, and Le Song. Learning temporal point processes via reinforcement learning. *Advances in Neural Information Processing Systems*, 31, 2018.
- [47] Yan Li, Tingjian Ge, and Cindy Chen. Data stream event prediction based on timing knowledge and state transitions. *Proceedings of the VLDB Endowment*, 13(10):1779–1792, 2020.
- [48] Yang Li. Reflection: enabling event prediction as an on-device service for mobile interaction. In *Proceedings of the 27th annual ACM symposium on User interface software and technology*, pages 689–698, 2014.
- [49] Yunqi Li, Hanxiong Chen, Zuohui Fu, Yingqiang Ge, and Yongfeng Zhang. User-oriented fairness in recommendation. In *Proceedings of the Web Conference 2021*, pages 624–632, 2021.
- [50] Bryan Lim. Forecasting treatment responses over time using recurrent marginal structural networks. *Advances in Neural Information Processing Systems*, 31, 2018.
- [51] Hongyuan Mei and Jason M Eisner. The neural Hawkes process: A neurally self-modulating multivariate point process. *Advances in Neural Information Processing Systems*, 30, 2017.

- [52] Valentyn Melnychuk, Dennis Frauen, and Stefan Feuerriegel. Causal transformer for estimating counterfactual outcomes. In *International Conference on Machine Learning*, pages 15293–15329. PMLR, 2022.
- [53] George Mohler. Marked point process hotspot maps for homicide and gun crime prediction in chicago. *International Journal of Forecasting*, 30(3):491–497, 2014.
- [54] George O Mohler, Martin B Short, P Jeffrey Brantingham, Frederic Paik Schoenberg, and George E Tita. Self-exciting point process modeling of crime. *Journal of the American Statistical Association*, 106(493):100–108, 2011.
- [55] Ashley I Naimi, Erica EM Moodie, Nathalie Auger, and Jay S Kaufman. Constructing inverse probability weights for continuous exposures: A comparison of methods. *Epidemiology*, 25(2):292–299, 2014.
- [56] Brady Neal. Introduction to causal inference. *Course Lecture Notes*, 2020.
- [57] Lizhen Nie, Mao Ye, Dan Nicolae, et al. VCNet and functional targeted regularization for learning causal effects of continuous treatments. In *International Conference on Learning Representations*, 2021.
- [58] Yosihiko Ogata. Space-time point-process models for earthquake occurrences. *Annals of the Institute of Statistical Mathematics*, 50:379–402, 1998.
- [59] Yosihiko Ogata and David Vere-Jones. Inference for earthquake models: A self-correcting model. *Stochastic Processes and Their Applications*, 17(2):337–347, 1984.
- [60] Thomas Opitz, Haakon Bakka, Raphaël Huser, and Luigi Lombardo. High-resolution Bayesian mapping of landslide hazard with unobserved trigger event. *The Annals of Applied Statistics*, 16(3):1653–1675, 2022.
- [61] Judea Pearl. Causal inference in statistics: An overview. *Statistics Surveys*, 3:96, 2009.
- [62] Judea Pearl et al. Models, reasoning and inference. *Cambridge University Press*, 19(2):3, 2000.
- [63] Gustavo Pereira. Recursive embedding and clustering. 2023.
- [64] Alex Reinhart. A review of self-exciting spatio-temporal point processes and their applications. *Statistical Science*, 33(3):299–318, 2018.
- [65] James Robins. A new approach to causal inference in mortality studies with a sustained exposure period—application to control of the healthy worker survivor effect. *Mathematical Modelling*, 7(9-12):1393–1512, 1986.
- [66] James M Robins. Correcting for non-compliance in randomized trials using structural nested mean models. *Communications in Statistics-Theory and Methods*, 23(8):2379–2412, 1994.

- [67] James M Robins. Association, causation, and marginal structural models. *Synthese*, 121(1/2):151–179, 1999.
- [68] James M Robins, Sander Greenland, and Fu-Chang Hu. Estimation of the causal effect of a time-varying exposure on the marginal mean of a repeated binary outcome. *Journal of the American Statistical Association*, 94(447):687–700, 1999.
- [69] James M Robins, Miguel Angel Hernan, and Babette Brumback. Marginal structural models and causal inference in epidemiology. *Epidemiology*, pages 550–560, 2000.
- [70] Donald B Rubin. Bayesian inference for causal effects: The role of randomization. *The Annals of Statistics*, pages 34–58, 1978.
- [71] Frederic Paik Schoenberg. Multidimensional residual analysis of point process models for earthquake occurrences. *Journal of the American Statistical Association*, 98(464):789–795, 2003.
- [72] Peter Schulam and Suchi Saria. Reliable decision support using counterfactual models. *Advances in Neural Information Processing Systems*, 30, 2017.
- [73] David W Scott. On optimal and data-based histograms. *Biometrika*, 66(3):605–610, 1979.
- [74] Qianqian Shan, Yili Hong, and William Q Meeker. Seasonal warranty prediction based on recurrent event data. *The Annals of Applied Statistics*, 14(2):929–955, 2020.
- [75] Marko Tkalcic, Matevz Kunaver, Andrej Kosir, and J Tasic. Addressing the new user problem with a personality based user similarity measure. In *The UMAP 2011 Workshops-DEMRA 2011 and UMMS 2011: Decision Making and Recommendation Acceptance Issues in Recommender Systems; User Models for Motivational Systems: The affective and the rational routes to persuasion*, volume 740, pages 106–111. CEUR-WS. org, 2011.
- [76] Yixin Wang, Dhanya Sridhar, and David M Blei. Equal opportunity and affirmative action via counterfactual predictions. *arXiv preprint arXiv:1905.10870*, 2019.
- [77] Ling Heng Wong, Philippa Pattison, and Garry Robins. A spatial model for social networks. *Physica A: Statistical Mechanics and its Applications*, 360(1):99–120, 2006.
- [78] Shenghao Wu, Wenbin Zhou, Minshuo Chen, and Shixiang Zhu. Counterfactual generative models for time-varying treatments. *arXiv preprint arXiv:2305.15742*, 2023.
- [79] Carl Yang, Xiaolin Shi, Luo Jie, and Jiawei Han. I know you'll be back: Interpretable new user clustering and churn prediction on a mobile social application. In *Proceedings of the 24th ACM SIGKDD International Conference on Knowledge Discovery & Data Mining*, pages 914–922, 2018.

- [80] Jinsung Yoon, James Jordon, and Mihaela Van Der Schaar. GANITE: Estimation of individualized treatment effects using generative adversarial nets. In *International Conference on Learning Representations*, 2018.
- [81] Qiang Zhang, Aldo Lipani, Omer Kirnap, and Emine Yilmaz. Self-attentive Hawkes process. In *International Conference on Machine Learning*, pages 11183–11193. PMLR, 2020.
- [82] Shixiang Zhu, Ruyi Ding, Minghe Zhang, Pascal Van Hentenryck, and Yao Xie. Spatio-temporal point processes with attention for traffic congestion event modeling. *IEEE Transactions on Intelligent Transportation Systems*, 23(7):7298–7309, 2021.
- [83] Shixiang Zhu and Yao Xie. Spatiotemporal-textual point processes for crime linkage detection. *The Annals of Applied Statistics*, 16(2):1151–1170, 2022.
- [84] Shixiang Zhu, Henry Shaowu Yuchi, and Yao Xie. Adversarial anomaly detection for marked spatio-temporal streaming data. In *ICASSP 2020-2020 IEEE International Conference on Acoustics, Speech and Signal Processing (ICASSP)*, pages 8921–8925. IEEE, 2020.
- [85] Shixiang Zhu, Minghe Zhang, Ruyi Ding, and Yao Xie. Deep Fourier kernel for self-attentive point processes. In *Proceedings of The 24th International Conference on Artificial Intelligence and Statistics*, volume 130, pages 856–864, 2021.
- [86] Hao Zou, Peng Cui, Bo Li, Zheyuan Shen, Jianxin Ma, Hongxia Yang, and Yue He. Counterfactual prediction for bundle treatment. In *Advances in Neural Information Processing Systems*, volume 33, pages 19705–19715, 2020.
- [87] Hao Zou, Bo Li, Jiangang Han, Shuiping Chen, Xuetao Ding, and Peng Cui. Counterfactual prediction for outcome-oriented treatments. In *Proceedings of the 39th International Conference on Machine Learning*, volume 162, pages 27693–27706, 2022.
- [88] Simiao Zuo, Haoming Jiang, Zichong Li, Tuo Zhao, and Hongyuan Zha. Transformer Hawkes process. In *International Conference on Machine Learning*, pages 11692–11702. PMLR, 2020.

A Derivation for temporal point processes

The conditional probability of point processes can be derived from the conditional intensity (1). Suppose we are interested in the conditional probability of events at a given point $x \in \mathcal{X}$, and we assume that there are i events that happen before $t(x)$. Let $\Omega(x)$ be a small neighborhood containing x . According to (1), we can rewrite $\lambda(x|\mathcal{H}_{t(x)})$ as following:

$$\begin{aligned}\lambda(x|\mathcal{H}_{t(x)}) &= \mathbb{E}(d\mathbb{N}(x)|\mathcal{H}_{t(x)})/dx = \mathbb{P}\{x_{i+1} \in \Omega(x)|\mathcal{H}_{t(x)}\}/dx \\ &= \mathbb{P}\{x_{i+1} \in \Omega(x)|\mathcal{H}_{t_{i+1}} \cup \{t_{i+1} \geq t(x)\}\}/dx \\ &= \frac{\mathbb{P}\{x_{i+1} \in \Omega(x), t_{i+1} \geq t(x)|\mathcal{H}_{t_{i+1}}\}/dx}{\mathbb{P}\{t_{i+1} \geq t(x)|\mathcal{H}_{t_{i+1}}\}}.\end{aligned}$$

Here $\mathcal{H}_{t_{i+1}} = \{x_1, \dots, x_i\}$ represents the history up to i -th events. If we let $F(t(x)|\mathcal{H}_{t(x)}) = \mathbb{P}(t_{i+1} < t(x)|\mathcal{H}_{t_{i+1}})$ be the conditional cumulative probability, and $f(x|\mathcal{H}_{t(x)}) \triangleq f(x_{i+1} \in \Omega(x)|\mathcal{H}_{t_{i+1}})$ be the conditional probability density of the next event happening in $\Omega(x)$. Then the conditional intensity can be equivalently expressed as

$$\lambda(x|\mathcal{H}_{t(x)}) = \frac{f(x|\mathcal{H}_{t(x)})}{1 - F(t(x)|\mathcal{H}_{t(x)})}.$$

We multiply the differential $dx = dt dm$ on both sides of the equation and integral over the mark space \mathcal{M} :

$$\begin{aligned}dt \cdot \int_{\mathcal{M}} \lambda(x|\mathcal{H}_{t(x)}) dm &= \frac{dt \cdot \int_{\mathcal{M}} f(x|\mathcal{H}_{t(x)}) dm}{1 - F(t(x)|\mathcal{H}_{t(x)})} = \frac{dF(t(x)|\mathcal{H}_{t(x)})}{1 - F(t(x)|\mathcal{H}_{t(x)})} \\ &= -d \log(1 - F(t(x)|\mathcal{H}_{t(x)})).\end{aligned}$$

Hence, integrating over t on $[t_i, t(x))$ leads to the fact that

$$\begin{aligned}F(t(x)|\mathcal{H}_{t(x)}) &= 1 - \exp\left(-\int_{t_i}^{t(x)} \int_{\mathcal{M}} \lambda(x|\mathcal{H}_{t(x)}) dm dt\right) \\ &= 1 - \exp\left(-\int_{[t_i, t(x)) \times \mathcal{M}} \lambda(x|\mathcal{H}_{t(x)}) dx\right)\end{aligned}$$

because $F(t_i) = 0$. Then we have

$$f(x|\mathcal{H}_{t(x)}) = \lambda(x|\mathcal{H}_{t(x)}) \cdot \exp\left(-\int_{[t_i, t(x)) \times \mathcal{M}} \lambda(x|\mathcal{H}_{t(x)}) dx\right),$$

which corresponds to (2).

The log-likelihood of one observed event series in (3) is derived, by the chain rule, as

$$\begin{aligned}\ell(x_1, \dots, x_{N_T}) &= \log f(x_1, \dots, x_{N_T}) = \log \prod_{i=1}^{N_T} f(x_i|\mathcal{H}_{t_i}) \\ &= \int_{\mathcal{X}} \log f(x|\mathcal{H}_{t(x)}) d\mathbb{N}(x) \\ &= \int_{\mathcal{X}} \log \lambda(x|\mathcal{H}_{t(x)}) d\mathbb{N}(x) - \int_{\mathcal{X}} \lambda(x|\mathcal{H}_{t(x)}) dx.\end{aligned}$$

The log-likelihood of K observed event sequences can be conveniently obtained with the counting measure \mathbb{N} replaced by the counting measure \mathbb{N}_k for the k -th sequence.

B Markov history process

The history embedding used by NPP defined in (4) can be regarded as a series of realizations of q -dimensional homogeneous Markov process [41]. Notably, the history $\mathcal{H}_{t(x)}$ in (5) is a *filtration* associated with the MTPP, which is a sequence of σ -algebras (or information sets) that satisfy $\mathcal{H}_s \subseteq \mathcal{H}_t$ for $s \leq t$, representing the accumulation of information up to the time t . Statistically, the history embedding $h(x)$ can be viewed as the realization of a q -dimensional random variable that effectively encapsulates the information contained in the filtration. To facilitate the explanation for the rest of the paper, the history embedding up to the i th event, or $h(x_i)$; and the one for the next unobserved event x , or $h(x)$, is denoted as h_i and h , respectively. It is important to note that while $h(x)$ and h can be continuously defined in \mathcal{X} , h_i is only constructed at the observed events. This paper investigates the relation between the history embedding h_i and h , and the corresponding intensity carefully to construct the counterfactual intensity framework. The proof of the Markov property is detailed below.

The history embedding is formulated as follows by (4):

$$h(x) = \phi(t(x) - t(x_n), m(x), h(x_n)).$$

Suppose the history variable $\mathcal{H}_t(x)$ contains the events x_1, x_2, \dots, x_n up to time $t(x)$, then we can obtain the following expressions from the equation above:

$$\begin{aligned} h_1 &:= h(x_1) = \phi(t(x_1), m(x_1), h_0); \\ h_{i+1} &:= h(x_{i+1}) = \phi(t(x_{i+1}) - t(x_i), m(x_{i+1}), h_i), \end{aligned}$$

for any integer $i > 0$. Since the mapping function $\phi(\cdot)$ for h_{i+1} is independent from h_0 up to h_{i-1} , we can reach the following deduction for the conditional probability:

$$p(h_{i+1}|h_0, h_1, \dots, h_i) = p(h_{i+1}|h_i),$$

for any non-negative integer i . Therefore, we may reach the expression for the joint probability function for history embedding:

$$\begin{aligned} p(h_0, h_1, h_2, \dots, h_n, h(x)) &= p(h_0)p(h_1|h_0)p(h_2|h_1, h_0) \dots p(h(x)|h_0, h_1, \dots, h_n) \\ &= p(h_0)p(h_1|h_0)p(h_2|h_1) \dots p(h_n|h_{n-1})p(h(x)|h_n). \end{aligned}$$

The conditional probability distribution then becomes

$$\begin{aligned} p(h(x)|h_0, h_1, \dots, h_n) &= \frac{p(h_0, h_1, h_2, \dots, h_n, h(x))}{p(h_0, h_1, h_2, \dots, h_n)} \\ &= \frac{p(h_0)p(h_1|h_0)p(h_2|h_1) \dots p(h_n|h_{n-1})p(h(x)|h_n)}{p(h_0)p(h_1|h_0)p(h_2|h_1) \dots p(h_n|h_{n-1})} \\ &= p(h(x)|h_n). \end{aligned}$$

Finally, the intensity function $\lambda(x|h(t))$ is conditional only on the history embedding $h(x)$ by (5), so by treating λ as a mapping we can reach

$$\lambda(x|h(x)) = \lambda(x|h(x), h_n, \dots, h_i, \dots, h_1, h_0).$$

C Proof of Lemma 2

The counterfactual probability density of MTPPs can be derived from the joint probability of discrete event x , history embedding h_i , and the cluster c . From the causal graph shown in Fig. 2, we can formulate the joint probability function $f(x, h, c)$ as follows:

$$f(x, h, c) = f(x|h, c) \cdot f(c) \cdot \prod_{\tau=1}^i f(h_\tau|h_{\tau-1}, c) \cdot f(h_0|c). \quad (18)$$

From the joint probability distribution, we can then derive the conditional distribution $f(x|h)$, or shorthanded as $f_h(x)$:

$$\begin{aligned} f_h(x) &= \int f(x|h, c) \cdot f(c) dc \\ &= \int f(x|h, c) \cdot \frac{\prod_{\tau=1}^i f(h_\tau|h_{\tau-1}, c)}{\prod_{\tau=1}^i f(h_\tau|h_{\tau-1}, c)} \cdot f(c) dc \\ &= \int \frac{1}{\prod_{\tau=1}^i f(h_\tau|h_{\tau-1}, c) f(h_0|c)} \left[f(x|h, c) \cdot \prod_{\tau=1}^i f(h_\tau|h_{\tau-1}, c) \cdot f(c) \cdot f(h_0|c) \right] dc. \end{aligned}$$

After reorganizing the conditional distribution $f_h(x)$, we plug in the expression for the joint distribution in (18):

$$f_h(x) = \int \frac{1}{\prod_{\tau=1}^i f(h_\tau|h_{\tau-1}, c) f(h_0|c)} f(x, h, c) dc.$$

In the setting of our problem, the initial history embedding h_0 starts where there have yet been any events observed at all. Therefore, $f(h_0|c)$ can be regarded as a constant of 1 since h_0 is independent from c and not random. This results in the following expression:

$$f_h(x) = \int \frac{1}{\prod_{\tau=1}^i f(h_\tau|h_{\tau-1}, c)} f(x, h, c) dc.$$

Finally, in this work the cluster $c \in \mathcal{C}$ is a discrete variable, so we modify to the discrete case and obtain the final expression:

$$f_h(x) = \sum_{c \in \mathcal{C}} \frac{1}{\prod_{\tau=1}^i f(h_\tau|h_{\tau-1}, c)} f(x, h, c),$$

arriving at (7) that reaches the lemma.

D Proof of Proposition 1

The learning objective function for weighted maximum log-likelihood estimation can be obtained via the definition of expectation. We twice expand the expectation with respect to $f(x|h)$ (or $f_h(x)$) and the event history variable h :

$$\begin{aligned} \mathbb{E}_h [\mathbb{E}_{x \sim f_h} [\log f_\theta(x|h)]] &= \mathbb{E}_h \left[\int \log f_\theta(x|h) \cdot f_h(x) dx \right] \\ &= \int \int \log f_\theta(x|h) \cdot f_h(x) \cdot f(h) dx dh \end{aligned}$$

The distribution of history embedding variable h is typically customized. In this work, we wish to treat each history variable equally, and combined with computational simplicity, we set $f(h) = 1$. Furthermore, using the expression of $f_h(x)$ in (7) from Lemma 2 while treating C as continuous, we obtain

$$\begin{aligned}\mathbb{E}_h [\mathbb{E}_{x \sim f_h} [\log f_\theta(x|h)]] &= \int \int \log f_\theta(x|h) \cdot \int \frac{1}{\prod_{\tau=1}^i f(h_\tau|h_{\tau-1}, c)} f(x, h, c) dcdx dh \\ &= \int \int \int \log f_\theta(x|h) \cdot \frac{1}{\prod_{\tau=1}^i f(h_\tau|h_{\tau-1}, c)} f(x, h, c) dcdx dh.\end{aligned}$$

Denote $1/\prod_{\tau=1}^i f(h_\tau|h_{\tau-1}, c)$ by $w(\bar{h}, c)$ and take the expectation with data tuple (x, h, c) , we then reach

$$\begin{aligned}\mathbb{E}_h [\mathbb{E}_{x \sim f_h} [\log f_\theta(x|h)]] &= \int \int \int \log f_\theta(x|h) w(\bar{h}, c) f(x, h, c) dh dcdx \\ &= \mathbb{E}_{(x, h, c)} [w(\bar{h}, c) \log f_\theta(x|h)] \\ &\approx \frac{1}{|\mathcal{D}|} \sum_{(x_i^{(k)}, \bar{h}_i^{(k)}, c) \in \mathcal{D}} w(\bar{h}_i^{(k)}, c) \log f_\theta(x_i^{(k)}|h_i^{(k)}), \\ &\propto \frac{1}{K} \sum_{(x_i^{(k)}, \bar{h}_i^{(k)}, c) \in \mathcal{D}} w(\bar{h}_i^{(k)}, c) \log f_\theta(x_i^{(k)}|h_i^{(k)}),\end{aligned}$$

which can be approximated by samples of data tuples $(x_i^{(k)}, \bar{h}_i^{(k)}, c)$ from the whole set \mathcal{D} , where $|\mathcal{D}|$ denotes the number of data tuples, thus arriving at the first half of (8).

The set \mathcal{D} of the data tuples $(x_i^{(k)}, \bar{h}_i^{(k)}, c)$ contains the history embedding trajectory for all K users, so we can restructure them by k :

$$\frac{1}{K} \sum_{(x_i^{(k)}, \bar{h}_i^{(k)}, c) \in \mathcal{D}} w(\bar{h}_i^{(k)}, c) \log f_\theta(x_i^{(k)}|h_i^{(k)}) = \frac{1}{K} \sum_{k=1}^K \sum_{i=1}^{N_T^{(k)}} w(\bar{h}_i^{(k)}, c) \log f_\theta(x_i^{(k)}|h_i^{(k)}).$$

Plug in the expressions for the probability density function from (2), we obtain:

$$\begin{aligned}&\frac{1}{K} \sum_{(x_i^{(k)}, \bar{h}_i^{(k)}, c) \in \mathcal{D}} w(\bar{h}_i^{(k)}, c) \log f_\theta(x_i^{(k)}|h_i^{(k)}) \\ &= \frac{1}{K} \sum_{k=1}^K \sum_{i=1}^{N_T^{(k)}} w(\bar{h}_i^{(k)}, c) \log \left(\lambda_\theta(x_i|h_i) \exp \left(- \int_{[t_{i-1}, t_i] \times \mathcal{M}} \lambda_\theta(x|h_i) dx \right) \right) \\ &= \frac{1}{K} \sum_{k=1}^K \sum_{i=1}^{N_T^{(k)}} w(\bar{h}_i^{(k)}, c) \left(\log \lambda_\theta(x_i|h_i) - \int_{[t_{i-1}, t_i] \times \mathcal{M}} \lambda_\theta(x|h_i) dx \right).\end{aligned}$$

We then plug in the log-likelihood function expression from (3):

$$\begin{aligned}
&= \frac{1}{K} \sum_{k=1}^K \left(\sum_{i=1}^{N_T^{(k)}} w(\bar{h}_i^{(k)}, c) \log \lambda_\theta(x_i | h_i) - \sum_{i=1}^{N_T^{(k)}} \int_{[t_{i-1}, t_i) \times \mathcal{M}} w(\bar{h}_i^{(k)}, c) \lambda_\theta(x | h_i) dx \right) \\
&= \left(\frac{1}{K} \sum_{k=1}^K \sum_{i=1}^{N_T^{(k)}} w(\bar{h}_i^{(k)}, c) \log \lambda_\theta(x_i | h_i) \right) - \left(\frac{1}{K} \sum_{k=1}^K \int_{\mathcal{X}} w(\bar{h}_n^{(k)}, c) \lambda_\theta(x | h^{(k)}) dx \right) \\
&= \frac{1}{K} \sum_{k=1}^K \int_{\mathcal{X}} w(\bar{h}, c) \log \lambda_\theta(x | h) d\mathbb{N}^{(k)}(x) - \frac{1}{K} \sum_{k=1}^K \int_{\mathcal{X}} w(\bar{h}_n^{(k)}, c) \lambda_\theta(x | h^{(k)}) dx \\
&= \frac{1}{K} \sum_{k=1}^K \left(\int_{\mathcal{X}} w(\bar{h}, c) \log (\lambda_\theta(x | h(x))) d\mathbb{N}^{(k)}(x) - \int_{\mathcal{X}} w(\bar{h}_n^{(k)}, c) \lambda_\theta(x | h^{(k)}(x)) dx \right),
\end{aligned}$$

finally arriving at the latter half of (8).

E Derivation of Lemma 3

In this analysis, we assume the variables h_i and h_{i-1} are scalars, but it can be easily extended to higher dimension. Looking into the joint probability of the tuple (h_i, h_{i-1}, c) , since c is a known categorical variable, we may omit it when deriving the probability $p(h_i, h_{i-1})$. Suppose there are m samples of the tuple (h_i, h_{i-1}) , and we wish to approximate the true joint probability distribution function of h_i and h_{i-1} , denoted by $f(h_i, h_{i-1})$, by approximation using binning. Suppose the probability of a sample falling in a particular bin is denoted by $p_m(h_i, h_{i-1})$ and the size of bins in h_i and h_{i-1} are uniform denoted by δ , we can express it as follows:

$$p_m(h_i, h_{i-1}) = \int_{t(h_i)}^{t(h_i) + \delta} \int_{t(h_{i-1})}^{h_{i-1} + \delta} f(x_i, x_{i-1}) dx_i dx_{i-1}, \quad (19)$$

where x_i denotes a variable in the domain of h_i , and x_{i-1} denotes a variable in the domain of h_{i-1} , $t(h_i)$ denotes the lower bound of the bin in h_i and $t(h_i) + \delta$ is then the upper bound, same with h_{i-1} .

We expand the expression in (19) using Taylor's expansion to the first degree which yields

$$\begin{aligned}
p_m(h_i, h_{i-1}) &= \int_{t(h_i)}^{t(h_i) + \delta} \int_{t(h_{i-1})}^{h_{i-1} + \delta} f(h_i, h_{i-1}) + \frac{\partial f(h_i, h_{i-1})}{\partial h_i} (x_i - h_i) \\
&\quad + \frac{\partial f(h_i, h_{i-1})}{\partial h_{i-1}} (x_{i-1} - h_{i-1}) + \mathcal{O}(\delta^2) dx_i dx_{i-1} \\
&= \delta^2 f(h_i, h_{i-1}) + \frac{1}{2} \frac{\partial f}{\partial h_i} [\delta^3 - 2\delta^2(x_i - t(h_i))] \\
&\quad + \frac{1}{2} \frac{\partial f}{\partial h_{i-1}} [\delta^3 - 2\delta^2(x_{i-1} - t(h_{i-1}))] + \mathcal{O}(\delta^4),
\end{aligned}$$

where $\mathcal{O}(\cdot)$ indicates higher order terms which are small in magnitude.

Now we denote $\nu_m(h_i, h_{i-1})$ as the number of samples falling in this bin, which therefore follows a binomial distribution (since a sample can either be within or without the bin), denoted by $\mathcal{B}\{m, p_m(h_i, h_{i-1})\}$. This leads to

$$\begin{aligned}\mathbb{E}[\nu_m] &= mp_m, \\ \text{Var}[\nu_m] &= mp_m(1 - p_m).\end{aligned}$$

Given ν_m , we can write out the estimator for the true probability density function \hat{f}_δ :

$$\hat{f}_\delta = \frac{\nu_m}{m\delta^2}.$$

We then thus express the expectation and variance of the estimator \hat{f}_δ :

$$\begin{aligned}\mathbb{E}[\hat{f}_\delta] &= \frac{\mathbb{E}[\nu_m]}{m\delta^2} = \frac{p_m(h_i, h_{i-1})}{\delta^2} \\ &= f(h_i, h_{i-1}) + \frac{1}{2} \frac{\partial f}{\partial h_i} [\delta - 2(x_i - t(h_i))] + \frac{1}{2} \frac{\partial f}{\partial h_{i-1}} [\delta - 2(x_{i-1} - t(h_{i-1}))] + \mathcal{O}(\delta^2); \\ \text{Bias} &= \frac{1}{2} \frac{\partial f}{\partial h_i} [\delta - 2(x_i - t(h_i))] + \frac{1}{2} \frac{\partial f}{\partial h_{i-1}} [\delta - 2(x_{i-1} - t(h_{i-1}))] + \mathcal{O}(\delta^2); \\ \text{Var}[\hat{f}_\delta] &= \frac{\text{Var}[\nu_m]}{m^2\delta^4} = \frac{p_m(1 - p_m)}{m\delta^4} \\ &= \frac{1}{m} \frac{1}{\delta^4} [f(h_i, h_{i-1})\delta^2 + \mathcal{O}(\delta^4)] [1 - \mathcal{O}(\delta^2)] \\ &= \frac{f(h_i, h_{i-1})}{m\delta^2} + \mathcal{O}(\frac{1}{m}).\end{aligned}$$

F Proof of Proposition 3

Following the results of Lemma 3, the mean square error for the estimator can be formulated as follows:

$$\begin{aligned}\text{MSE} &= \text{Bias}^2 + \text{Var} \\ &= \frac{f(h_i, h_{i-1})}{m\delta^2} + \mathcal{O}(\frac{1}{m}) + \mathcal{O}(\delta^3) \\ &\quad + \frac{1}{4} (\frac{\partial f}{\partial h_i})^2 \delta^2 + (\frac{\partial f}{\partial h_i})(h_i - t(h_i))^2 + \frac{1}{4} (\frac{\partial f}{\partial h_{i-1}})^2 \delta^2 + (\frac{\partial f}{\partial h_{i-1}})(h_{i-1} - t(h_{i-1}))^2 \\ &\quad - \delta (\frac{\partial f}{\partial h_i})^2 (h_i - t(h_i)) - \delta (\frac{\partial f}{\partial h_{i-1}})^2 (h_{i-1} - t(h_{i-1})) + \frac{1}{2} \frac{\partial f}{\partial h_i} \frac{\partial f}{\partial h_{i-1}} \delta^2 \\ &\quad + 2 \frac{\partial f}{\partial h_i} \frac{\partial f}{\partial h_{i-1}} (h_i - t(h_i))(h_{i-1} - t(h_{i-1})) - \delta \frac{\partial f}{\partial h_i} \frac{\partial f}{\partial h_{i-1}} (h_{i-1} - t(h_{i-1})) \\ &\quad - \delta \frac{\partial f}{\partial h_i} \frac{\partial f}{\partial h_{i-1}} (h_i - t(h_i)).\end{aligned}$$

Now we make the assumption here that the number of events in the sequence is long enough, such that we expect the joint distribution of the embedding between two steps $f(h_i, h_{i-1})$ to be symmetric between h_i and h_{i-1} since the transition behavior is

expected to converge. Then we can argue that the two partial derivatives are equivalent in magnitude given the and can be denoted so:

$$\frac{\partial f}{\partial h_i} = \frac{\partial f}{\partial h_{i-1}} = f'.$$

Now taking the integral over (x_i, x_{i-1}) , the integrated mean square error (IMSE) can be found by taking the two-dimensional integral of all the terms in MSE. The first few terms are straightforward to integrate:

$$\int_{t(h_i)}^{t(h_i)+\delta} \int_{t(h_{i-1})}^{t(h_{i-1})+\delta} \frac{f(h_i, h_{i-1})}{m\delta^2} + \mathcal{O}\left(\frac{1}{m}\right) + \mathcal{O}(\delta^3) dh_i dh_{i-1} = \frac{1}{m\delta^2} + \mathcal{O}\left(\frac{1}{m}\right) + \mathcal{O}(\delta^5).$$

The next four terms can be derived directly:

$$\begin{aligned} \int \int \frac{1}{4} \left(\frac{\partial f}{\partial h_i} \right)^2 \delta^2 dh_i dh_{i-1} &= \frac{1}{4} \delta^3 \int \left(\frac{\partial f}{\partial h_i} \right)^2 dh_i = \frac{1}{4} \delta^3 \int f'^2, \\ \int \int \left(\frac{\partial f}{\partial h_i} \right) (h_i - t(h_i))^2 dh_i dh_{i-1} &= \frac{1}{3} \delta^3 \int f'^2 + \mathcal{O}(\delta^3); \\ \int \int \delta \left(\frac{\partial f}{\partial h_i} \right)^2 (h_i - t(h_i)) dh_i dh_{i-1} &= \frac{1}{2} \delta^3 \int f'^2 + \mathcal{O}(\delta^3); \\ \int \int \frac{1}{2} \frac{\partial f}{\partial h_i} \frac{\partial f}{\partial h_{i-1}} \delta^2 dh_i dh_{i-1} &= \frac{1}{2} \delta^2 \left(\int f' \right)^2 + \mathcal{O}(\delta^3). \end{aligned}$$

The derivation of the final two terms requires the use of the assumption on the two partial derivatives:

$$\begin{aligned} 2 \frac{\partial f}{\partial h_i} \frac{\partial f}{\partial h_{i-1}} (h_i - t(h_i))(h_{i-1} - t(h_{i-1})) \\ &= 2 \int \frac{\partial f}{\partial h_i} (h_i - t(h_i)) \int \frac{\partial f}{\partial h_{i-1}} (h_{i-1} - t(h_{i-1})) dh_{i-1} \\ &= 2 \left(\frac{1}{2} \delta^2 \int \frac{\partial f}{\partial h_i} dh_i \right) \left(\frac{1}{2} \delta^2 \int \frac{\partial f}{\partial h_{i-1}} dh_{i-1} \right) + \mathcal{O}(\delta^5) \\ &= \frac{1}{2} \delta^4 \left(\int f' \right)^2 + \mathcal{O}(\delta^5). \end{aligned}$$

The final term can be derived in a similar way:

$$\begin{aligned} \delta \frac{\partial f}{\partial h_i} \frac{\partial f}{\partial h_{i-1}} (h_{i-1} - t(h_{i-1})) \\ &= \delta \int \frac{\partial f}{\partial h_i} dh_i \int \frac{\partial f}{\partial h_{i-1}} (h_{i-1} - t(h_{i-1})) dh_{i-1} \\ &= \delta \int \frac{\partial f}{\partial h_i} dh_i \left(\frac{1}{2} \delta^2 \int \frac{\partial f}{\partial h_{i-1}} dh_{i-1} + \mathcal{O}(\delta^3) \right) \\ &= \frac{1}{2} \delta^3 \int \frac{\partial f}{\partial h_i} dh_i \int \frac{\partial f}{\partial h_{i-1}} dh_{i-1} + \mathcal{O}(\delta^4) \\ &= \frac{1}{2} \delta^3 \left(\int f' \right)^2 + \mathcal{O}(\delta^4). \end{aligned}$$

When put together, the IMSE can be expressed as

$$\text{IMSE} = \frac{1}{m\delta^2} + \frac{1}{2}\delta^2 \left(\int f' \right)^2 + \mathcal{O}(\delta^3) + \mathcal{O}\left(\frac{1}{m}\right).$$

To obtain the best value of δ^* , we set the derivative of IMSE to 0 dropping the higher order terms and solve the equation.

$$\frac{-2}{m\delta^3} + \delta \left(\int f' \right)^2 = 0 \Rightarrow \delta^* = \left(\frac{2}{\left(\int f' \right)^2} \right)^{1/4} m^{-1/4}.$$

Therefore, we have reached the approximate estimator of the optimal bin size δ^* which minimizes the IMSE caused by bin discretization. This applies when $\int f' \neq 0$.

In the event where $\int f' = 0$, the IMSE is formulated differently:

$$\begin{aligned} \text{IMSE} &= \frac{1}{m\delta^2} + \left(\frac{1}{4} + \frac{1}{3} + \frac{1}{4} + \frac{1}{3} - \frac{1}{2} - \frac{1}{2} \right) \delta^3 \int f'^2 + \mathcal{O}(\delta^4) \\ &= \frac{1}{6} \delta^3 \int f'^2 + \mathcal{O}(\delta^4). \end{aligned}$$

We similarly take the derivative to find the optimal δ .

$$\frac{-2}{m\delta^3} + \frac{1}{2} \delta^2 \int f'^2 = 0 \Rightarrow \delta^* = \left(\frac{4}{\int f'^2} \right)^{1/5} m^{-1/5}.$$

G More results on conditional transition probability

The conditional transition probabilities are visualized in Fig. 3 with $1/\delta = 20$ bins. Here we provide two extra sets of visualizations with different number of bins in Fig. 6 and 7. They illustrate how the patterns change as δ changes.

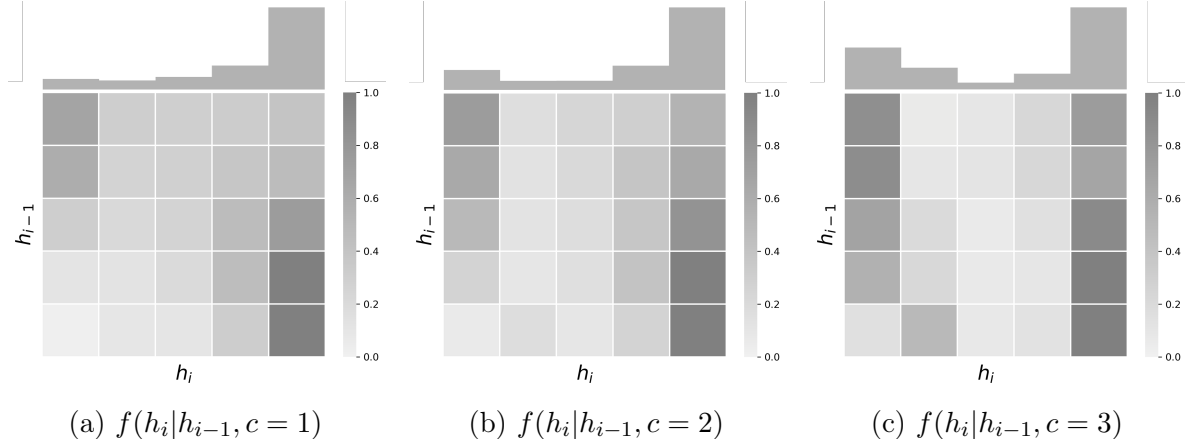


Figure 6: The histogram of $p(h_i|c)$ and the conditional transition probability $p(h_i|h_{i-1}, c)$ in three categories $c = 1, 2, 3$ when $1/\delta = 5$. We can visually identify the difference of the conditional histogram and transition probability under different user category c .

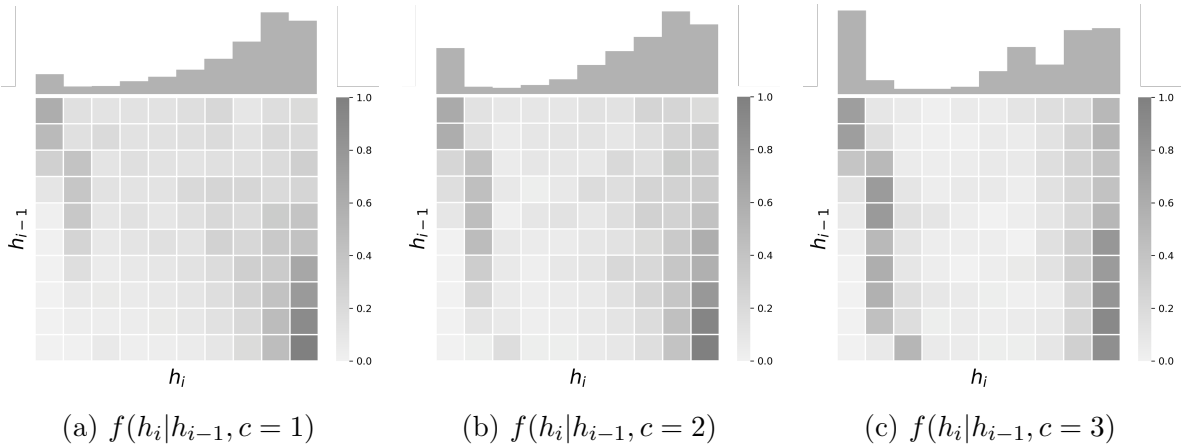


Figure 7: The histogram of $p(h_i|c)$ and the conditional transition probability $p(h_i|h_{i-1}, c)$ in three categories $c = 1, 2, 3$ when $1/\delta = 10$. We can visually identify the difference of the conditional histogram and transition probability under different user category c .

H Details for simulation study

We investigate a number of synthetic experiments in this study, which we summarize first below and then expand for details.

1. Three categories each generate 400 event sequences for the training set, and an additional 100 for the testing one. Sequences within the same category is generated by a temporal Hawkes point process model with exponential triggering function and parameters fixed. Hidden embedding dimension is set to $q = 1$ and the number of bins $1/\delta = 25$, number of epochs $\eta = 5$.
2. We keep the same setting for the Hawkes models of the three categories, but composition of event sequences from each category is no longer balanced. There are now 200 sequences generated by the first Hawkes model, 400 by the second, and 600 by the third one, thereby creating an unbalanced dataset between three categories.
3. Composition is further changed. Now 600 sequences are now generated by the first Hawkes model, 400 by the second, and 200 by the third one. This is another unbalanced training set.
4. Three Hawkes processes for the three categories with parameters no longer fixed. The 1,200 sequences are evenly divided between categories, but the parameter values are drawn from fixed random variables when sampling for each sequence. Event sequences in each category observe a different yet still similar behavior.
5. We utilize different families of point process models for the three categories. For the first and the second categories, we still utilize two exponential Hawkes process with different parameter. For the third category, we elect to use a Neural Hawkes model. Each category still contributes 400 training and 100 testing sequences.
6. We look into more complex event data with an additional mark variable, *i.e.* the marked point process. We append an additional discrete mark variable to the

event sequences generated. We utilize three marked-temporal Hawkes processes for simulation, each contributing the same number of sequences.

H.1 Synthetic experiment 1-3

In this scenario, the event sequences are generated from three independent Hawkes point processes with the exponential kernel function, each corresponding to sequences within a user cluster. Temporal Hawkes point processes without marks utilize the following conditional intensity function:

$$\lambda_g(t|\mathcal{H}_t) = \mu + \int_0^t g(t-u)d\mathbb{N}(u) = \mu + \sum_{i:t_i < t} g(t-t_i), \quad (20)$$

where μ is the constant background rate variable, and $g(\cdot)$ is the triggering function that determines the form of self-excitation [64]. Since $\lambda(t|\mathcal{H}_t)$ is non-negative, $g(u) \geq 0$ for $u \geq 0$ and $g(u) = 0$ otherwise. Here we designate the triggering function to take the exponential form

$$g(t-t_i) = \alpha \cdot \exp(-\beta(t-t_i)). \quad (21)$$

In this scenario, we fix $\mu = 0.1$, $\alpha = 1$, and alter β to generate event sequences of different patterns. For each of the three temporal Hawkes point process models we use to generate the event sequences, we set $\beta = 0.5$, 1.0 , and 1.5 respectively. Thereby we generate 400 sequences from each of the three PPs in the time range of $T \in [0, 100]$, and the training set contains 1,200 event sequences coming from the three clusters, divided evenly between them such that each cluster contains 400 event sequences. For the testing dataset, we obtained 100 user sequences from each Hawkes PP instead with cluster information removed, a total of 300 sequences. Therefore, we get 111,499 events in the training set, and 15,974 in the testing set, which is sufficiently large. For evaluation, their cluster information is masked so the testing sequences are regarded as coming from "new" users. We construct our models with weights upon NH and RMTPP models, where the dimension of hidden variables is set to $q = 1$ given the relatively simple mechanism. We partition this 1D embedding space into $S = 25$ bins of equal size to obtain the conditional history transition probabilities when deriving the IPTW values for our framework.

Following the simulation setting, we obtain the MAE values for each of the 100 testing sequences drawn from their corresponding exponential Hawkes PP. We look into the comparison between the Neural Hawkes model and the Weighted NH with the proposed reweighting scheme applied more carefully. From Table 1, we can see that the Weighted NH does better than NH overall in terms of MAE, by roughly 11%. The Weighted RMTPP does better as well, by 3%.

Additionally, we study the impact on the proposed framework and the baseline methods by different testing data compositions from the three clusters in the testing set. This corresponds to the situation where the composition of event sequences in the training set is different from that in the testing set. We investigate two of such scenarios, denoted by Exp. 2 and 3, respectively. Both of them still entail 1,200 training sequences split evenly from the same three exponential Hawkes PP model, but the composition of their testing set changes. For Synthetic Exp. 2, the numbers of testing event sequences generated by the three Hawkes PP models are 50, 100, and 150 respectively. While

for Synthetic Exp. 3, the numbers of testing sequences are 150, 100, and 50 instead. Configurations during training remain the same. The quantitative results are also included in Table 1. The results suggest that in both cases, the proposed methods better predict performance than the baseline models. Specifically, for the comparison between NH and the Weighted NH methods, the improvement in the two scenarios is by 5% and 10%, respectively. The improvement over the RMTPP model using our method is 2.4% and 3.1%, respectively. This demonstrates that our proposed framework indeed can carry out predictions more accurately for users with event patterns less observed, even when the data composition is imbalanced.

H.2 Synthetic experiment 4

In the previous section, we look into the case where event sequences in the same cluster are generated from the same PP model. However, in reality, things are usually less ideal. The pattern of events within the same cluster is likely to be similar, but rarely identical. In this scenario, we look into the situation where the event sequences within the same cluster are no longer drawn from the same fixed PP model, yet still they are relatively similar to each other in the cluster.

Instead of a Hawkes process with a constant fixed β for each cluster, we now consider β as a random variable, which is sampled randomly whenever an event sequence is simulated. This way, the pattern of event sequences within the cluster will be similar, but no longer identical, creating a more complex and realistic dataset for the cluster. To differentiate between the three clusters, in this case, we define the random variable β for each cluster as follows:

$$\begin{aligned} C_1 : \quad \beta &\in \mathcal{U}[0.4, 0.6]; \\ C_2 : \quad \beta &\in \mathcal{U}[0.9, 1.1]; \\ C_3 : \quad \beta &\in \mathcal{U}[1.4, 1.6], \end{aligned}$$

which indicates the β are uniform random variables in their respective ranges for each cluster. This more complex event sequence generation for each cluster applies to both the 1,200 training sequences and the 300 testing sequences. The other configurations stay the same, and we can obtain the MAE results in Table 1. We can see that between the MAE from NH and Weighted NH, the latter has a lower MAE by 12%, which suggests our proposed model works better than baselines in this scenario. For RMTPP, the improvement is about 9%.

H.3 Synthetic experiment 5

So far the PP models used in event sequence generation are all exponential Hawkes PP. In this scenario, we study the situation where event sequences are drawn from different distribution families. For the first two clusters in this experiment, we continue to draw event sequences from exponential Hawkes PP, with $\beta = 0.5$ and 1 , respectively. However, for the third cluster in this case, we utilize an individual Neural Hawkes PP model with parameters randomly set to generate both training and testing event sequences. We set the hidden variable dimension to two when generating sequences from the NH model, which produces 400 training sequences and an additional 100 testing sequences for the third cluster.

Therefore, the total number of event sequences drawn from the three clusters remains the same. When we train our models and the baselines, the dimension of hidden variables is set to $q = 3$, higher than the dimension used in generation. We partition this 3D embedding space into $1/\delta^3 = 5^3 = 125$ bins of equal size for the conditional history transition. The MAE results for all the methods are logged again in Table 1. We see that for both NH and RMTPP models, our proposed framework improves their performance in the weighted counterpart by 3% and 10% respectively. It demonstrates our framework can well handle the situation where the event sequence pattern is no longer identical within the same cluster.

H.4 Synthetic experiment 6

In this synthetic experiment, we study the case where event sequence data contain an additional categorical mark variable on top of the time component. Marked temporal event data are common in real applications, making this study relevant. In this scenario, the conditional intensity function is constructed as follows:

$$\lambda(t, m|\mathcal{H}_t) = \lambda_g(t|\mathcal{H}_t)f(m|t), \quad (22)$$

where $\lambda_g(t|\mathcal{H}_t)$ is the conditional intensity for the temporal Hawkes PP as in (20), and the mark component is defined by $f(m|t)$ dependent on time only. It can be described using probability mass functions.

$$\begin{aligned} f(m=1|t) &= \begin{cases} 0.8, & \text{if } t \leq 40, \\ 0, & \text{otherwise,} \end{cases} \\ f(m=2|t) &= \begin{cases} 0.8, & \text{if } 40 < t \leq 80, \\ 0, & \text{otherwise,} \end{cases} \\ f(m=0|t) &= \begin{cases} 0.2, & \text{if } t \leq 80, \\ 1, & \text{otherwise.} \end{cases} \end{aligned}$$

Therefore, the event sequences in this scenario are still first drawn from exponential Hawkes PPs and then appended with the additional mark, which can only take values between $(0, 1, 2)$. Given the introduction of an additional mark variable, we again set the dimension of the hidden variable to $q = 3$, and the number of bins to $S = 125$. The numerical results are appended in Table 1. For a more detailed breakdown on MAE values across different categories in the testing set, the results are illustrated in Fig. 4.

From the results, we can see our weighted methods generally perform better than the baselines. Comparing NH and C-NH, we see the MAE from the proposed weighted method is lower by 4%. For RMTPP, the improvement is 2.3%. It indicates our proposed method can improve prediction performance for marked TPP models, and will likely work well in real case studies.

To summarize the simulations studies, we have shown throughout the section including multiple data configurations that the application of our proposed reweighting scheme can consistently and robustly improve the prediction performance of the common PP models utilizing the hidden variables.